



# Face Gear Drive With Spur Involute Pinion: Geometry, Generation by a Worm, Stress Analysis

Faydor L. Litvin, Alfonso Fuentes, Claudio Zanzi, and Matteo Pontiggia  
University of Illinois at Chicago, Chicago, Illinois

## The NASA STI Program Office . . . in Profile

Since its founding, NASA has been dedicated to the advancement of aeronautics and space science. The NASA Scientific and Technical Information (STI) Program Office plays a key part in helping NASA maintain this important role.

The NASA STI Program Office is operated by Langley Research Center, the Lead Center for NASA's scientific and technical information. The NASA STI Program Office provides access to the NASA STI Database, the largest collection of aeronautical and space science STI in the world. The Program Office is also NASA's institutional mechanism for disseminating the results of its research and development activities. These results are published by NASA in the NASA STI Report Series, which includes the following report types:

- **TECHNICAL PUBLICATION.** Reports of completed research or a major significant phase of research that present the results of NASA programs and include extensive data or theoretical analysis. Includes compilations of significant scientific and technical data and information deemed to be of continuing reference value. NASA's counterpart of peer-reviewed formal professional papers but has less stringent limitations on manuscript length and extent of graphic presentations.
- **TECHNICAL MEMORANDUM.** Scientific and technical findings that are preliminary or of specialized interest, e.g., quick release reports, working papers, and bibliographies that contain minimal annotation. Does not contain extensive analysis.
- **CONTRACTOR REPORT.** Scientific and technical findings by NASA-sponsored contractors and grantees.

- **CONFERENCE PUBLICATION.** Collected papers from scientific and technical conferences, symposia, seminars, or other meetings sponsored or cosponsored by NASA.
- **SPECIAL PUBLICATION.** Scientific, technical, or historical information from NASA programs, projects, and missions, often concerned with subjects having substantial public interest.
- **TECHNICAL TRANSLATION.** English-language translations of foreign scientific and technical material pertinent to NASA's mission.

Specialized services that complement the STI Program Office's diverse offerings include creating custom thesauri, building customized data bases, organizing and publishing research results . . . even providing videos.

For more information about the NASA STI Program Office, see the following:

- Access the NASA STI Program Home Page at <http://www.sti.nasa.gov>
- E-mail your question via the Internet to [help@sti.nasa.gov](mailto:help@sti.nasa.gov)
- Fax your question to the NASA Access Help Desk at 301-621-0134
- Telephone the NASA Access Help Desk at 301-621-0390
- Write to:  
NASA Access Help Desk  
NASA Center for Aerospace Information  
7121 Standard Drive  
Hanover, MD 21076



# Face Gear Drive With Spur Involute Pinion: Geometry, Generation by a Worm, Stress Analysis

Faydor L. Litvin, Alfonso Fuentes, Claudio Zanzi, and Matteo Pontiggia  
University of Illinois at Chicago, Chicago, Illinois

Prepared under Grant NAG3-2450

National Aeronautics and  
Space Administration

Glenn Research Center

## Acknowledgments

The authors express their deep gratitude to the Army Research of Office, NASA Glenn Research Center, and Gleason Foundation for the financial support of the research project.

Available from

NASA Center for Aerospace Information  
7121 Standard Drive  
Hanover, MD 21076

National Technical Information Service  
5285 Port Royal Road  
Springfield, VA 22100

Available electronically at <http://gltrs.grc.nasa.gov/GLTRS>

# Face Gear Drive with Spur Involute Pinion: Geometry, Generation by a Worm, Stress Analysis

Faydor L. Litvin, Alfonso Fuentes, Claudio Zanzi, Matteo Pontiggia  
Gear Research Center, Department of Mechanical Engineering  
University of Illinois at Chicago  
Chicago, Illinois 60607

## Abstract

A face gear drive with a spur involute pinion is considered. The generation of the face gear is based on application of a grinding or cutting worm whereas the conventional method of generation is based on application of an involute shaper. An analytical approach for determination of: (i) the worm thread surface, (ii) avoidance of singularities of the worm thread surface, (iii) dressing of the worm, and (iv) determination of stresses of the face-gear drive, is proposed. A computer program for simulation of meshing and contact of the pinion and face-gear has been developed. Correction of machine-tool settings is proposed for reduction of the shift of the bearing contact caused by misalignment. An automatic development of the model of five contacting teeth has been proposed for stress analysis. Numerical examples for illustration of the developed theory are provided.

## Nomenclature

$\alpha_c$	Pressure angle for symmetric face-gear drive for driving and coast sides
$\Delta\gamma$	Change of shaft angle
$\Delta E$	Change of shortest distance between the pinion and the face-gear axes
$\Delta q$	Axial displacement of face gear
$\lambda_w$	Crossing angle between axes of shaper and worm
$\gamma_m$	Shaft angle
$\eta_s$	Half of the width of the space on the base cylinder
$\Sigma_i (i = s, 1, 2, w)$	Tooth surface of the shaper ( $i = s$ ), of the pinion ( $i = 1$ ), of the face-gear ( $i = 2$ ), of the generating worm ( $i = w$ )
$\psi_i (i = s, 2, w)$	Angle of rotation of the shaper ( $i = s$ ), of the face gear ( $i = 2$ ) and of the worm ( $i = w$ ) applied for the process of generation
$\theta_s, u_s$	Surface parameters

$E_{sw}$	Shortest distance between the axes of the shaper and the worm
$L_i (i = 1, 2)$	Inner ( $i = 1$ ) and outer ( $i = 2$ ) limiting dimensions of the face gear
$l_w$	Translational motion of the worm in the process of the generation of the face-gear
$\mathbf{M}_{ji}, \mathbf{L}_{ji}$	Matrices 4×4 and 3×3 for transformation from $S_i$ to $S_j$ of point coordinates and projections of vectors
$N_i (i = s, 1, 2, w)$	Number of teeth of the shaper ( $i = s$ ), of the pinion ( $i = 1$ ), of the face-gear ( $i = 2$ ), of the generating worm ( $i = w$ )
$P_d$	Diametral pitch
$r_{ps}$	Radius of the pitch circle of the shaper
$r_{p1}$	Radius of the pitch circle of the pinion
$r_{bs}$	Radius of the base cylinder

# 1. Introduction

A face gear drive with intersected axes formed by a spur pinion and conjugated face gear is considered. The advantages of application of face gear drives in helicopter transmissions (Fig.1) are the possibility of the split of the torque and reduction of weight. The existing design of face gear drives is based on application of an involute spur pinion of the drive. A substantial step in the technology of face-gear drives is the development of grinding (and hobbing) of face gears by a grinding worm (a hob, respectively) [14].

The contents of the paper cover:

- (1) A brief summary of the existing geometry and output of TCA (Tooth Contact Analysis) computer program developed for simulation of meshing and contact.
- (2) Concept of generation of face-gears by grinding or cutting worm, analytical derivation of worm thread surface, its dressing and avoidance of undercutting of the worm generated by the shaper.
- (3) Stress analysis of face-gear drives. A model with five contacting teeth is developed automatically.

The performed research is based on application of modern theory of gearing that has been a subject of research by V. A. Zalgaller [21], [22], N. Stosik [18], [19], [20], G. Bar [4], G. I. Shevelova [16], Baumann [3], Stadtfeld [17] and F. L. Litvin and his followers [1], [2], from [7] to [13]. The developed theory is illustrated with numerical examples.

## 2. Geometry of Existing Design

**Generation of Face-Gear.** The conventional method of generation of the face-gear is based on application of an involute shaper. The process of generation is based on simulation of meshing of the face-gear with the involute shaper. The authors have considered as well a prospective method for generation of the face-gear by a worm that might be applied as a grinding worm or a hob (section 3).

**Localization of Contact.** Localization of the bearing contact between the tooth surfaces of the involute pinion and the face gear is achieved as follows:

1. The face-gear may be determined as the envelope to the family of surfaces of an involute shaper with tooth number  $N_s > N_p$  where  $N_s$  and  $N_p$  are the tooth numbers of the shaper and the pinion of the drive. Usually,  $N_s - N_p = 2 \Leftrightarrow 3$ .
2. The pinion and the shaper of the drive are in an imaginary internal tangency as shown in Fig. 2.
3. We may consider that three surfaces  $\Sigma_s$ ,  $\Sigma_2$  and  $\Sigma_1$  are in mesh simultaneously. The surfaces of the shaper  $\Sigma_s$  and the face-gear  $\Sigma_2$  are in line tangency at every instant. However, surface  $\Sigma_2$  and pinion surface  $\Sigma_1$  are in tangency at a point at every instant since  $N_p < N_s$ .

**Structure of Face Gear Tooth.** The tooth surfaces  $\Sigma_2$  of the face-gear generated by an involute shaper are shown in Fig. 3(a). Lines  $L_{2S}$  represent the instantaneous lines of tangency of  $\Sigma_2$  and shaper  $\Sigma_s$  shown on  $\Sigma_2$ . The cross-sections of the face-gear tooth are shown in Fig. 3(b). Investigation shows that the surface points of the face-gear are hyperbolic ones. This means that the product of principal curvatures at the surface point is negative. The fillet of the face-gear tooth surface of a conventional design (Fig. 3) is generated by the edge of the shaper. The authors have proposed to generate the fillet by a rounded edge of the shaper as shown in Fig. 4 that allows the bending stresses to be reduced approximately in 10%. The shape of the modified fillet of the face gear is shown in Fig. 5.

The length of the face-gear teeth has to be limited by dimensions  $L_1$  and  $L_2$  (Fig. 6) to avoid [8]: (i) undercutting in plane A, and (ii) tooth pointing in plane B. The permissible length of the face-gear tooth is determined by the unit less coefficient  $c$  represented as

$$c = (L_2 - L_1)P_d = \frac{L_2 - L_1}{m} \quad (1)$$

where  $P_d$  and  $m$  are the diametral pitch and the module, respectively. The magnitude of coefficient  $c$  depends mainly on the gear ratio  $m_{12} = \frac{N_2}{N_1}$  and is usually in the range  $8 < c < 15$ .

**Results of TCA (Tooth Contact Analysis).** TCA is designated for simulation of meshing and contact of surfaces  $\Sigma_1$  and  $\Sigma_2$  and permits the investigation of the influence of errors of alignment on transmission errors and the shift of bearing contact. The TCA algorithm is based on observation of continuous tangency of pinion and face-gear tooth surfaces  $\Sigma_1$  and  $\Sigma_2$  (See details in [8]). Application of the TCA program indicates: (i) errors of alignment do not cause transmission errors, but (ii) cause the shift of bearing contact. The advantage of zero transmission errors is the result of application of an involute pinion that has equidistant profiles.

The sensitivity of the bearing contact of the face gear drive to errors of alignment requires special corrections to obtain a central location of the bearing contact. It has been proven that this can be obtained by axial displacement  $\Delta q$  of the face-gear with respect to the pinion.

The investigation is based on application of coordinate systems shown in (Figs. 7 and 8). Coordinate systems  $S_1$  and  $S_f$  are rigidly connected to the pinion and the frame of the face-gear drive, respectively (Fig. 7(a)). To simulate the misalignment of the face-gear, we use auxiliary coordinate systems  $S_q$  (Fig. 7(b)),  $S_d$  and  $S_e$  (Fig. 8(a)). The location of  $S_q$  with respect to  $S_f$  is shown in Fig. 7(b). Parameters  $\Delta E$ ,  $B$  and  $B \cot \gamma$  determine the location of the origin  $O_q$  with respect to  $O_f$ . Here,  $\Delta E$  is the shortest distance between the pinion and the face-gear axes when the axes are crossed but not intersected; parameters  $B$  and  $B \cot \gamma$  are shown in Fig. 7(b).

Auxiliary fixed coordinate systems  $S_q$ ,  $S_d$  and  $S_e$  are shown in Fig. 8(a). The face-gear performs rotation about the  $z_e$  axis (Fig. 8(b)). The location of  $S_e$  with respect to  $S_d$  simulates the axial displacement  $\Delta q$  of the face-gear (Fig. 8(b)). The orientation of  $S_d$  with respect to  $S_q$  simulates the installment of the crossing angle  $\gamma = \gamma_m + \Delta\gamma$ , where  $\gamma_m$  is the shaft angle, and  $\Delta\gamma$  is caused by the misalignment (Fig. 8(a)).

### Numerical Example 1.

The output of TCA has been obtained for a face gear drive with the following data:

$$\text{Pinion tooth number } N_1 = 25$$

$$\text{Face gear tooth number } N_2 = 160$$

$$\text{Shaper tooth number } N_s = 28$$

$$\text{Crossing angle } \gamma_m = 90^\circ$$

$$\text{Pressure angle } \alpha_c = 25^\circ .$$

Fig. 9 shows: (i) the bearing contact of aligned gear drive (Fig. 9(a)), and (ii) the shift of bearing contact caused by errors  $\Delta\gamma$  and  $\Delta E$  (Figs. 9(b) and 9(c)). Fig. 10 shows that the location of the bearing contact is restored by axial displacement  $\Delta q$  of the face gear.

## 3. Application of Generating Worm

**Concept of Generating Worm.** The conventional method for generation of a face-gear is based on:

- (i) Application of an involute shaper, and
- (ii) Manufacturing of face-gear based on simulation of meshing of the shaper and the face-gear being generated.

Edward W. Miller has proposed in 1942 the generation of the face-gear by a hob [15]. The rational part of his patent was the idea of consideration of internal meshing of the hob with the pinion of the face-gear drive. However, the patent did not provide the necessary conditions of conjugation of the tooth surfaces of the hob, the pinion, and the face-gear, directions of worm design, and avoidance of worm singularities. Therefore, undercutting of the face-gear and impermissible deviations of the face-gear tooth surface from the theoretical one could not be avoided.

The next step was done by the patent proposed by Litvin et al. [14] that has provided the exact determination of the thread surface of a generating worm that might be applied for grinding and cutting of face-gears.

This paper covers the solution to the following problems of the design of a grinding worm:

1. Determination of crossing angle between the axes of the shaper and the worm
2. Determination of worm thread surfaces
3. Avoidance of singularities of the worm thread surface
4. Dressing of worm thread surface

**Crossing Angle Between Axes of Shaper and Worm.** Fig. 11 shows fixed coordinate systems  $S_a$ ,  $S_b$  and  $S_c$  applied for illustration of installment of the worm with respect to the shaper. Moveable coordinate systems  $S_s$  and  $S_w$  are rigidly connected to the shaper and the worm. Axis  $z_s$  (it coincides with  $z_a$ ) is the axis of rotation of the

shaper. Axis  $z_w$  (it coincides with  $z_c$ ) is the axis of rotation of the worm. Axes  $z_s$  and  $z_w$  are crossed and form a crossing angle  $90^\circ \pm \lambda_w$ . The upper (and lower) sign corresponds to application of a right-hand (left-hand) worm. The shortest distance between axes  $z_s$  and  $z_w$  is designated as  $E_{ws}$ .

The derivation of crossing angle  $\lambda_w$  is based on observation of simultaneous tangency of surfaces  $\Sigma_s$ ,  $\Sigma_2$ ,  $\Sigma_w$ . For the purpose of simplification of derivations, we consider the tangency of those surfaces that are equidistant to  $\Sigma_s$ ,  $\Sigma_2$  and  $\Sigma_w$  and pass through point  $P$  determined in  $S_a$  as (Figs. 11 and 12)

$$\mathbf{r}_a^{(P)} = [r_{ps} \quad 0 \quad 0]^T \quad (2)$$

where  $r_{ps}$  is the radius of the pitch circle of the shaper.

The derivation of crossing angle  $\lambda_w$  is based on the following procedure:

*Step 1:* We consider initially the tangency at P of surfaces that are equidistant to  $\Sigma_s$  and  $\Sigma_2$ . Axes  $z_s$  and  $z_2$  of rotation of the shaper and the face-gear are intersected (Fig. 12), and therefore there is an instantaneous axis of rotation  $O_s I$  that passes through intersection point  $O_m$  [8]. Point P is chosen on  $O_m I$ . Tangency of surfaces  $\Sigma_s$  and  $\Sigma_2$  is provided because the normals to  $\Sigma_s$  pass through point P (Figs. 12, 15).

*Step 2:* Tangency of surfaces  $\Sigma_s$  and  $\Sigma_w$  at point P is observed, if the following equation of meshing between  $\Sigma_s$  and  $\Sigma_w$  is satisfied at P [8].

$$\mathbf{N}^{(s)} \cdot \mathbf{v}^{(sw)} = 0 \quad (3)$$

Here:  $\mathbf{N}^{(s)}$  is the normal to  $\Sigma_s$ ; vector  $\mathbf{v}^{(sw)}$  is determined as  $\mathbf{v}^{(sw)} = \mathbf{v}^{(s)} - \mathbf{v}^{(w)}$ , where  $\mathbf{v}^s$  and  $\mathbf{v}^w$  are the velocities of point  $P$  of the shaper and the worm.

Using equation (3), we obtain after derivations that

$$\lambda_w = \arcsin \frac{r_{ps}}{N_s (E_{ws} + r_{ps})} \quad (4)$$

Here:  $r_{ps}$  is the pitch radius of the shaper, and  $E_{ws}$  (Fig. 11) is the shortest distance between the axes of the shaper and the worm. The magnitude of  $E_{ws}$  affects the dimensions of the grinding worm and the conditions of avoidance of surface singularities of the worm (see below). The meshing of the worm and the shaper is schematically illustrated in Fig. 13.

#### **Analytical Consideration of Simultaneous Meshing of Surfaces $\Sigma_s$ , $\Sigma_w$ and $\Sigma_2$ .**

Designations  $\Sigma_s$ ,  $\Sigma_w$  and  $\Sigma_2$  indicate surfaces of the shaper, worm and face-gear, respectively.

Simultaneous meshing of  $\Sigma_s$ ,  $\Sigma_w$  and  $\Sigma_2$  is illustrated by Fig. 14.

Shaper surface  $\Sigma_s$  is considered as a given generating one. Surfaces  $\Sigma_w$  and  $\Sigma_2$  are generated as the envelopes to the family of a shaper surface  $\Sigma_s$ .

### Determination of $\Sigma_w$ .

*Step 1:* Shaper surface  $\Sigma_s$  is represented as an involute surface of a spur gear (Fig. 15) determined by the equations

$$\begin{cases} x_s = r_{bs} [\cos(\theta_s + n_s) + \theta_s \sin(\theta_s + n_s)] \\ y_s = r_{bs} [\pm \sin(\theta_s + n_s) \mp \theta_s \cos(\theta_s + n_s)] \\ z_s = u_s \end{cases} \quad (5)$$

Here  $u_s$  and  $\theta_s$  are surface parameters; parameter  $n_s$  determines half of the width of the space on the base cylinder;  $r_{bs}$  is the radius of the base cylinder. Parameters  $\theta_s$  and  $n_s$  are shown in Fig. 15; parameter  $u_s$  is directed along the  $z_s$ -axis. The upper and lower signs in equation of  $y_s(\theta_s)$  correspond to profiles I and II, respectively.

*Step 2:* The worm surface  $\Sigma_w$  is determined in coordinate system  $S_w$  (Fig. 11) by the following equations [8]

$$\mathbf{r}_w(u_s, \theta_s, \psi_s) = \mathbf{M}_{ws}(\psi_s) \mathbf{r}_s(u_s, \theta_s) \quad (6)$$

$$\left( \frac{\partial \mathbf{r}_w}{\partial u_s} \times \frac{\partial \mathbf{r}_w}{\partial \theta_s} \right) \cdot \frac{\partial \mathbf{r}_w}{\partial \psi_s} = f_{ws}(u_s, \theta_s, \psi_s) = 0 \quad (7)$$

Here: vector function  $\mathbf{r}_w(u_s, \theta_s, \psi_s)$  is the family of shaper surfaces  $\Sigma_s$  represented in  $S_w$ ; matrix  $\mathbf{M}_{ws}(\psi_s)$  describes coordinate transformation from  $S_s$  to  $S_w$ ; equation (7) is the equation of meshing between  $\Sigma_s$  and  $\Sigma_w$ . Parameters  $(u_s, \theta_s)$  in vector function  $\mathbf{r}_w(u_s, \theta_s, \psi_s)$  represent the surface parameters of the shaper; parameter  $\psi_s$  in  $\mathbf{r}_w(u_s, \theta_s, \psi_s)$  is the generalized parameter of motion. As a reminder, that during generation of the worm the shaper and the worm perform rotations about crossed axes  $z_a$  and  $z_w$  (Fig. 11). Angles of rotation  $\psi_s$  and  $\psi_w$  (Fig. 11) are related by the equation

$$\frac{\psi_s}{\psi_w} = \frac{1}{N_s} \quad (8)$$

where  $N_s$  is the number of teeth of the shaper. It is assumed that a one-thread worm is applied. Figure 13 shows a schematic illustration of meshing of the shaper and the worm.

Equation of meshing (7) may be represented as well as [7], [8], [9].

$$\mathbf{N}_s \cdot \mathbf{v}_s^{(sw)} = f_{ws}(u_s, \theta_s, \psi_s) = 0 \quad (9)$$

Vector function  $\mathbf{r}_w(u_s, \theta_s, \psi_s)$  and equation of meshing  $f_{ws}(u_s, \theta_s, \psi_s) = 0$  represent the worm thread surface  $\Sigma_w$  by three related parameters. Surface  $\Sigma_w$  may be represented in form of two parameters by using the theorem of implicit function systems existence [6], [21].

Assume that equation of meshing  $f_{ws} = 0$  is satisfied at a point  $M(u_s^{(0)}, \theta_s^{(0)}, \psi_s^{(0)})$  and at this point we have that  $\frac{\partial f_{ws}}{\partial \theta_s} \neq 0$ . Then equation  $f_{ws}(u_s, \theta_s, \psi_s) = 0$  may be solved in the neighborhood of  $M$  by a function of class  $C^1$  as

$$\theta_s = \theta_s(u_s, \psi_s) \quad (10)$$

and the worm thread surface  $\Sigma_w$  may be determined locally as

$$\mathbf{r}_w(u_s, \theta_s(u_s, \psi_s), \psi_s) = \mathbf{R}_w(u_s, \psi_s) \quad (11)$$

### Determination of $\Sigma_2$

*Step 1:* The derivation of the face-gear surface  $\Sigma_2$  is based on the following considerations:

- (i) The shaper and the face-gear perform rotations about intersected axes  $z_s$  and  $z_2$  that form angle  $\gamma_m$  in a non-orthogonal face-gear drive (Fig. 12). Rotations of the shaper and face-gear are performed in a fixed coordinate system  $S_m$ ;  $z_m$  is the designation of the axis of rotation of the face-gear (Fig. 12).
- (ii) Face-gear tooth surface  $\Sigma_2$  is determined in coordinate system  $S_2$  by the following equations

$$\mathbf{r}_2(u_s, \theta_s, \psi_s) = \mathbf{M}_{2s}(\psi_s) \mathbf{r}_s(u_s, \theta_s) \quad (12)$$

$$\left( \frac{\partial \mathbf{r}_2}{\partial u_s} \times \frac{\partial \mathbf{r}_2}{\partial \theta_s} \right) \cdot \frac{\partial \mathbf{r}_2}{\partial \psi_s} = f_{2s}(u_s, \theta_s, \psi_s) = 0 \quad (13)$$

Here, parameters of vector function  $\mathbf{r}_2(u_s, \theta_s, \psi_s)$  designate surface parameters  $(u_s, \theta_s)$ , of the shaper and generalized parameter of motion  $\psi_s$ . The angles of rotation of the shaper,  $\psi_s$ , and the face-gear,  $\psi_2$ , are related as:

$$\frac{\psi_s}{\psi_2} = \frac{N_2}{N_s} \quad (14)$$

where  $N_s$  and  $N_2$  are the teeth numbers of the shaper and the face gear, respectively.

Equation (12) represents in coordinate system  $S_2$  the family of shaper surfaces  $\Sigma_s$ . Matrix  $\mathbf{M}_{2s}$  provides coordinate transformation from coordinate system  $S_s$  to  $S_2$ . Equation (13) is the equation of meshing between  $\Sigma_s$  and  $\Sigma_2$  of the shaper and the face-gear. An alternative form of equation of meshing, similar to equation (9), might be applied as well.

*Step 2:* It follows from the previous discussions that the shaper surface  $\Sigma_s$  is in line contact with the worm surface  $\Sigma_w$  and the face-gear tooth surface  $\Sigma_2$ . Such type of surface contact is obtained because  $\Sigma_w$  and  $\Sigma_2$  are generated as

envelope of shaper surface  $\Sigma_s$ . We designate by  $L_{sw}$  the line of tangency between  $\Sigma_s$  and  $\Sigma_w$  and by  $L_{s2}$  the line of tangency between  $\Sigma_s$  and  $\Sigma_2$ .

Investigation of lines  $L_{sw}$  and  $L_{s2}$  shows that they do not coincide with each other but are intersected at any position of meshing. Figs. 16(a) and fig16(b) show lines of tangency  $L_{sw}$  and  $L_{s2}$  that are functions of  $\psi_s$  and are represented in plane of parameters  $(u_s, \theta_s)$ . Fig.16(c) shows that lines  $L_{sw}(\psi_s^{(i)})$  and  $L_{s2}(\psi_s^{(i)})$  intersect with each other at a position of meshing  $\psi_s = \psi_s^{(i)}$ . The point of intersection of  $L_{sw}(\psi_s^{(s)})$  and  $L_{s2}(\psi_s^{(s)})$  corresponds to the point of tangency of surfaces  $\Sigma_w$  and  $\Sigma_2$ .

Vector function  $\mathbf{r}_2(u_s, \theta_s, \psi_s)$  and equation of meshing (13) represent surface  $\Sigma_2$  by three related parameters. Using the theorem of implicit function system existence, we may represent the face-gear tooth surface  $\Sigma_2$  in form of two parameters but locally as it was done for surface  $\Sigma_w$  (see representation of vector equations (11)).

**Generation of Surface  $\Sigma_2$  by Worm Surface  $\Sigma_w$ .** Remembering that the shaper surface  $\Sigma_s$  is in line contact with worm surface  $\Sigma_w$  and with face-gear tooth surface  $\Sigma_2$ , however, surfaces  $\Sigma_w$  and  $\Sigma_2$  are in point contact with each other at any instant. This means that finishing grinding of  $\Sigma_2$  by worm surface  $\Sigma_w$  cannot be accomplished. A grinding process based on related rotations of the worm and the face-gear will provide on  $\Sigma_2$  only a strip as the set of points of tangency of  $\Sigma_w$  and  $\Sigma_2$ . Therefore generation of  $\Sigma_2$  by the worm has to be based on a two-parameter enveloping process whereas two independent sets of parameters are provided as: (i) a set of angles of rotation  $(\psi_w, \psi_2)$  of the worm and the face-gear, and (ii) a translational motion  $l_w$  of the worm. Parameters  $\psi_w$  and  $\psi_2$  are the angles of rotation of the worm and the face-gear related by the equation:

$$\frac{\psi_w}{\psi_2} = \frac{N_2}{N_w} \quad (15)$$

where  $N_2$  and  $N_w$  are the number of teeth of the face-gear and the number of threads of the worm. Usually one-thread of worm is applied and  $N_w = 1$ .

Parameter  $l_w$  of translational motion is provided as collinear to the axis of the shaper (see below).

The following coordinate systems are applied for derivation of the face gear surface:

- (i) Fixed coordinate system  $S_b$  and  $S_c$  where we consider the rotation of the worm (Figs. 11 and 14)
- (ii) Fixed coordinate system  $S_m$  where we consider the rotation of the face-gear (Fig. 12)
- (iii) Movable coordinate system  $S_w$  rigidly connected to the worm (Fig. 11) and coordinate system  $S_2$  rigidly connected to the face-gear.

Surface  $\Sigma_2$  of the face-gear generated by the worm is determined by the following equations [7], [8], [21]:

$$\mathbf{r}_2(u_s, \theta_s, \psi_w, l_w) = \mathbf{M}_{2w}(\psi_w, l_w) \mathbf{r}_w(u_s, \theta_s(u_s, \psi_s), \psi_s) \quad (16)$$

$$\left[ \left( \frac{\partial \mathbf{r}_2}{\partial u_s} + \frac{\partial \mathbf{r}_2}{\partial \theta_s} \frac{\partial \theta_s}{\partial u_s} \right) \times \left( \frac{\partial \mathbf{r}_2}{\partial \psi_s} + \frac{\partial \mathbf{r}_2}{\partial \theta_s} \frac{\partial \theta_s}{\partial \psi_s} \right) \right] \cdot \frac{\partial \mathbf{r}_2}{\partial \psi_w} = 0 \quad (17)$$

$$\left[ \left( \frac{\partial \mathbf{r}_2}{\partial u_s} + \frac{\partial \mathbf{r}_2}{\partial \theta_s} \frac{\partial \theta_s}{\partial u_s} \right) \times \left( \frac{\partial \mathbf{r}_2}{\partial \psi_s} + \frac{\partial \mathbf{r}_2}{\partial \theta_s} \frac{\partial \theta_s}{\partial \psi_s} \right) \right] \cdot \frac{\partial \mathbf{r}_2}{\partial l_w} = 0 \quad (18)$$

Here, vector function

$$\mathbf{r}_w(u_s, \theta_s(u_s, \psi_s), \psi_s) = \mathbf{R}_w(u_s, \psi_s) \quad (19)$$

represents the worm surface. Function  $\theta_s(u_s, \psi_s)$  is obtained from equation of meshing (7) by using the theorem of implicit function system existence. Matrix  $\mathbf{M}_{2w}(\psi_w, l_w)$  represents the coordinate transformation from  $S_w$  to  $S_2$ . Vector function  $\mathbf{r}_2(u_s, \theta_s, \psi_w, l_w)$  represents in coordinates system  $S_2$  the family of worm surfaces  $\Sigma_w$ . Equations (17) and (18) represent the two equations of meshing of the two parameter enveloping process of generation. The cross-product of vectors in equations (17) and (18) represents in coordinate system  $S_2$  the normal to the worm surface.

Vectors  $\frac{\partial \mathbf{r}_2}{\partial \psi_w}$  and  $\frac{\partial \mathbf{r}_2}{\partial l_w}$  are equivalent to the relative velocities for generation of two sets of independent motions.

The generated surface  $\Sigma_2$  of the face-gear is covered by two families of contact lines I and II that correspond to  $l_w \neq \text{const}, \psi_w = \text{const}$  (Fig. 17(a)) and  $\psi_w \neq \text{const}, l_w = \text{const}$  (Fig. 17(b)), respectively. Instantaneous point  $M$  of tangency of worm and face-gear tooth surface is the point of intersection of lines I and II (Fig. 17(c)). The derivations performed above have resulted two versions of equations of face-gear tooth surface  $\Sigma_2$ : (i) equations from (16) to (18) that correspond to generation of  $\Sigma_2$  by the worm, and (ii) equations (12) and (13) that correspond to generation of  $\Sigma_2$  by the shaper. Certainly, the computation of  $\Sigma_2$  by the mentioned equations will provide the same numerical results.

**Avoidance of Singularities of Worm Thread Surface.** The worm thread surface has to be designed as a *regular* one. Surface point  $M$  is a singularity one if the surface normal is equal to zero at  $M$ . Determination of surface singularities is a complex problem for a surface represented by three related parameters, such as the worm thread surface (see equations (6) and (7)). We use in the upcoming discussions the following designations:  $\Sigma_w$  for the three-parameter surface, and  $\Sigma_s$  for the tool surface that generates  $\Sigma_w$ . Surface  $\Sigma_w$  is the envelope to the family of surfaces  $\Sigma_s$ .

Two alternative approaches for determination of singularities of surface  $\Sigma_w$  might be applied:

- (i) The first one (proposed by Zalgaller [21], [22]) is based on direct determination of normal  $\mathbf{N}_w$  to surface  $\Sigma_w$ .

- (ii) The second approach is based on consideration of tool surface  $\Sigma_s$  instead of  $\Sigma_w$  (proposed by Litvin [8]). The main goal of the second approach is to simplify derivations since  $\Sigma_s$  is a two parameter surface. The main idea of the approach is to determine initially those regular points on  $\Sigma_s$  that generate singular points on  $\Sigma_w$ .

The singularity equation in first approach is represented as

$$\left( \frac{\partial \mathbf{r}_w}{\partial \theta_s} \times \frac{\partial \mathbf{r}_w}{\partial \psi_s} \right) \frac{\partial f_{ws}}{\partial u_s} + \left( \frac{\partial \mathbf{r}_w}{\partial \psi_s} \times \frac{\partial \mathbf{r}_w}{\partial u_s} \right) \frac{\partial f_{ws}}{\partial \theta_s} + \left( \frac{\partial \mathbf{r}_w}{\partial u_s} \times \frac{\partial \mathbf{r}_w}{\partial \theta_s} \right) \frac{\partial f_{ws}}{\partial \psi_s} = \mathbf{0} \quad (20)$$

Here, vector function  $\mathbf{r}_w(u_s, \theta_s, \psi_s)$  is determined from equation (6);  $f_{ws}(u_s, \theta_s, \psi_s) = 0$  is the equation of meshing (7).

The second approach is based on the following considerations:

- (1) It is proven that surface singularity occurs if the following equation is observed [8]

$$\mathbf{v}_r^{(s)} + \mathbf{v}_r^{(sw)} = \mathbf{0} \quad (21)$$

Here:  $\mathbf{v}_r^{(s)}$  is the velocity of a point that moves over the tool surface  $\Sigma_s$ ;  $\mathbf{v}_r^{(sw)}$  is the relative sliding velocity in meshing of surfaces  $\Sigma_s$  and  $\Sigma_w$ . Vectors of equation (21) are represented in coordinate system  $S_s$ .

- (2) We apply in addition to equation (21) the differentiated equation of meshing (7) of the worm and the shaper. Then we obtain:

$$\frac{\partial f_{ws}}{\partial u_s} \frac{du_s}{dt} + \frac{\partial f_{ws}}{\partial \theta_s} \frac{d\theta_s}{dt} + \frac{\partial f_{ws}}{\partial \psi_s} \frac{d\psi_s}{dt} = 0 \quad (22)$$

- (3) Applications of equations (21) and (22) results in a system of four linear equations in two unknowns. The system has a certain solution for the unknowns if the matrix

$$\mathbf{A} = \begin{bmatrix} \frac{\partial \mathbf{r}_s}{\partial u_s} & \frac{\partial \mathbf{r}_s}{\partial \theta_s} & -\mathbf{v}_s^{(sw)} \\ \frac{\partial f_{ws}}{\partial u_s} & \frac{\partial f_{ws}}{\partial \theta_s} & \frac{\partial f_{ws}}{\partial \psi_s} \frac{d\psi_s}{dt} \end{bmatrix} \quad (23)$$

has the rank  $r = 2$ . This results in an equation

$$F_{ws}(u_s, \theta_s, \psi_s) = 0 \quad (24)$$

- (4) Equation of meshing (7) and equation (24) permits the sought-for line on  $\Sigma_s$  to be obtained that generates singular points on surface  $\Sigma_w$ .

The computational procedure for the determination and avoidance of worm singularities is as follows:

*Step 1:* Using equation of meshing (7), we are able to determine the lines of contact of the shaper and the worm in the plane of shaper parameters  $(u_s, \theta_s, \psi_s)$  as functions of the generalized parameter  $\psi_s$ . Fig. 18 illustrates such lines for both sides of shaper space.

*Step 2:* Using equation (24), we may determine the image of worm singular points in plane  $(u_s, \theta_s, \psi_s)$  (Fig. 18).

*Step 3:* Using equations (7) and (24) and equations of the shaper tooth surface, we may determine the lines of shaper regular points that generate the worm singularities.

*Step 4:* Using coordinate transformation from the shaper surface to the worm thread surface, we may determine: (i) regular points A on the shaper surface (Fig. 19(a)), and (ii) singularity points B on worm surface (Fig. 19(b)) that are generated by points A. Only one line of worm singularity points is represented in Fig. 19(b) due to limitations of rotation angle of the worm.

Singularities of the worm may be avoided by limitation of worm threads as shown in Fig. 19(b).

**Dressing of the Worm.** The worm dressing is based on generation of its surface  $\Sigma_w$  point by point by a plane or by a conical disk that has the same profile that the rack-cutter that generated the shaper. The execution of motions of the disk or the plane with respect to the worm is accomplished by application of a CNC machine. The determination of instantaneous installments of the grinding disk with respect to the worm requires application of a computer program. The algorithm of the program is based on the following considerations:

(1) The worm thread surface  $\Sigma_w$  is determined as the envelope to the family of shaper surfaces as follows:

$$\mathbf{r}_w = \mathbf{r}_w(u_s, \theta_s, \psi_s), \quad f_{ws}(u_s, \theta_s, \psi_s) = 0 \quad (25)$$

Equations (25) represent the worm surface by three related parameters

(2) The worm thread surface  $\Sigma_w$  may be represented in two parameter form using the theorem of implicit function

system existence as it was discussed above (see vector function (19)). Assume that  $\frac{\partial f_{ws}}{\partial \theta_s} \neq 0$ , at a point  $M(u_s^{(0)}, \theta_s^{(0)}, \psi_s^{(0)})$ . Then equation (7) may be solved in the neighborhood of  $M$  by

$$\theta_s = \theta_s(u_s, \psi_s) \in C^1 \quad (26)$$

and the worm surface may be represented as

$$\mathbf{r}_w(u_s, \theta_s(u_s, \psi_s), \psi_s) \quad (27)$$

The computational procedure is as follows:

*Step 1:* Take  $\theta_s = \text{constant}$ .

*Step 2:* Assign  $u_s$  and obtain  $\psi_s$  from  $\theta_s = \theta_s(u_s, \psi_s)$ .

*Step 3:* Compute  $x_w, y_w, z_w$  from

$$\mathbf{r}_w(u_s, \theta_s(u_s, \theta_s), \psi_s) \quad (28)$$

Step 4: Knowing  $u_s$ , it is easy to get  $\mathbf{n}_s(u_s)$  and then determine

$$\mathbf{n}_w(u_s, \theta_s, \psi_s) = \mathbf{L}_{ws}(\theta_s, \psi_s) \mathbf{n}_s(u_s) \quad (29)$$

Step 5: The data  $(x_w, y_w, z_w, \mathbf{n}_w)$  is sufficient for the installment of the tool (a plane or a disk) using a CNC machine.

**Numerical example.** The worm design parameters considered for this example are represented in Table 1.

Table 1: Design parameters of grinding worm

Direction of Worm Thread	Right Hand
Number of Worm Thread	$N_w = 1$
Number of teeth of the shaper	$N_s = 30$
Number of teeth of the face gear	$N_2 = 140$
Module	$m = 3.175 \text{ mm}$
Driving side pressure angle	$\alpha_c = 27.5^\circ$
Coast side pressure angle	$\alpha_c = 27.5^\circ$
Shaft angle	$\gamma_m = 100.0^\circ$
Worm Lead Angle	$\lambda_w = 0.786^\circ$
Shaft Distance between the Shaper and the Worm	$E_{ws} = 68.069 \text{ mm}$

The numerical values represented in Table 2 are obtained considering  $u_s = 0$ ;  $\theta_{\min} \leq \theta_s \leq \theta_{\max}$  and equations (7) and (24)

Table 2: Numerical values

Point	$u_s$	$\theta_s$	$\psi_s$	$N_{wx}$	$N_{wy}$	$N_{wz}$
1		0.701176	-0.232969	-0.359304	0.290277	0.886927
2		0.607726	-0.139518	0.242689	-0.393017	0.886927
3	0	0.514275	-0.046068	-0.098599	0.451263	0.886927
4		0.420824	0.047383	-0.056653	-0.458422	0.886927
5		0.327374	0.140833	0.205491	0.413683	0.886927

Here  $\psi_s$  is the angle of rotation of the shaper,  $N_{wx}$ ,  $N_{wy}$  and  $N_{wz}$  are the components of the normal to the worm surface in the worm coordinate system  $S_w$  at point  $M^{(i)}$ .

The minimum and the maximum values of  $\theta_s$  correspond respectively to the bottom and top of the shaper, calculated with the following equations:

$$\theta_i = \sqrt{\left(\frac{r_i}{r_{bs}}\right)^2} - 1 \quad i = (\max, \min) \quad (30)$$

For the considered numerical example the first singularity point (Fig. 18) occurs when  $\psi_s$  reaches the value  $\psi_s = 18.3^\circ$ . Such a point is located at the bottom of the thread of the worm as shown in Fig. 19(b). This is the maximum value for  $\psi_s$  that allows to generate a worm with *regular* points only. The corresponding worm rotation angle is  $\psi_w = 549^\circ$  that corresponds to  $549 / 360 = 1.5$  threads of the worm. Considering the two limitations for both sides, we obtain 3.0 as the maximum number of threads.

## 4. Stress Analysis

**Introduction** The goals of stress analysis represented in this section are:

- (i) Comparison of bending stresses at the fillet of two versions of face gear design: of the edged and rounded fillets (Fig. 4).
- (ii) Determination of contact and bending stresses and investigation of formation of the bearing contact during the cycle of meshing.

The performed stress analysis is based on finite element method [23] and application of general purpose computer program [5]. Finite element method [23] requires the development of a finite element mesh, definition of slave and master contacting surfaces and establishment of boundary conditions.

The authors' approach for application of finite element analysis has the following advantages:

- (a) The generation of finite element models is performed automatically by using the equations of the tooth surfaces and taking into account the corresponding fillets and portion of the rim. Loss of accuracy due to the development of solid models by using CAD computer programs is avoided.
- (b) The proposed approach does not require an assumption of load distribution in the contact area. The contact algorithm of the general purpose computer program [5] is used to get the contact area and stresses by application of the torque to the pinion. The gear is considered at rest.
- (c) Finite element models are developed numerically at the chosen contact point of the path of contact. Stress convergence is assured because there is at least one point of contact between the contacting surfaces.
- (d) Finite element models of five pairs of teeth are applied and therefore the boundary conditions are far enough from the loaded areas of the teeth.

**Development of Finite Element Models.** The development of finite element models using CAD computer programs is time expensive, requires skilled users for application of computer programs and has to be done for every case of development of gear geometry and the position of meshing desired for investigation. The approach developed is free of all these disadvantages and is summarized as follows:

*Step 1:* Using the equations of both sides of tooth surfaces and the portions of the corresponding rim, we may represent analytically the volume of the designed body. Fig. 20(a) shows the designed body for one-tooth model of the pinion of a face-gear drive.

*Step 2:* Auxiliary intermediate surfaces 1 to 6 as shown in Fig. 20(b) can be determined. Surfaces 1 to 6 divide the tooth in six parts and control the discretization of these tooth subvolumes into finite elements.

*Step 3:* Analytical determination of node coordinates is performed taking into account the number of desired elements in longitudinal and profile directions (Fig. 20(c)). We emphasize that all nodes of the finite element mesh are determined analytically and the points of intermediate surfaces of the tooth belong to the real gear tooth surfaces.

*Step 4:* Discretization of the model by finite elements (using the nodes determined in previous step) is accomplished as shown in Fig. 20(d).

*Step 5:* Setting of boundary conditions for the gear and the pinion are accomplished automatically under the following conditions:

- (i) Nodes on the two sides and bottom part of the portion of the gear rim are considered as fixed (Fig. 21(a))
- (ii) Nodes on the two sides and the bottom part of the pinion rim form a rigid surface (Fig. 21(a) and 21(b)). Such rigid surfaces are three-dimensional structures that may perform translation and rotation but cannot be deformed.
- (iii) The advantage of consideration of pinion rim rigid surfaces mentioned above is as follows: (a) their variables of motion (its translation and rotation) are associated with a single point chosen as the reference point  $M$  ; (b) point  $M$  is located on the pinion axis of rotation (Fig. 21(b)); (c) reference point  $M$  has only one degree-of-freedom (rotation about the pinion axis) and all other degrees-of-freedom are fixed; (d) the torque  $T$  in rotational motion is applied directly to the pinion at its reference node  $M$  (Fig. 21(b))

*Step 6:* The contact algorithm of the finite element analysis computer program [5] requires definition of contacting surfaces. The proposed approach identifies automatically all the elements of the model required for the formation of such surfaces.

The contact algorithm requires as well definition of master and slave surfaces. Generally, the choosing of a master surface is based on the following considerations [5]: (i) it is the surface of the stiffer body of the model, or (ii) the surface with coarser mesh if the contacting surfaces are located on structures with comparable stiffness. We have chosen for stress analysis the gear and pinion tooth surfaces as the master and slave ones, respectively.

**Numerical Example.** The finite element analysis has been performed for two versions of face gear drives of common design parameters represented in Table 3. The versions correspond to face gear drives with conventional and rounded fillet, respectively (Fig.4)

Table 3: Design parameters of face gear drive

Number of teeth of the pinion	25
Number of teeth of the shaper	28
Number of teeth of the face gear	160
Gear ratio	6.4
Module	6.35 mm
Driving side pressure angle	25.0 deg
Coast side pressure angle	25.0 deg
Shaft angle $\gamma_m$	90.0 deg
Inner radius of the face gear	471.0 mm
Outer radius of the face gear	559.0 mm

The finite element mesh of five-pair of teeth of version 2 is represented in Fig. 22. Elements [5] of first order enhanced by incompatible modes to improve their bending behavior have been used to form the finite element mesh.

The total number of elements is 67240 with 84880 nodes. The material is steel with the properties of Young's Modulus  $E = 2.068 \times 10^8 \text{ mN/mm}^2$  and Poisson's ratio 0.29. A torque of 1600 N·m has been applied to the pinion for both versions of face gear drives. Fig. 23 shows the model of the gear drive applied for stress analysis.

Figs. 24 and 25 show the maximum contact and bending stresses obtained at the mean contact point for gear drives of two versions of fillet (see Fig. 4). It is confirmed that the bending stresses are reduced more than 10% for the face-gear with a rounded fillet in comparison to the fillet generated by the edge of the shaper.

The stress analysis performed has been complemented with investigation of formation of the bearing contact (Figs. 25 and 26). The results obtained show the possibility of an edge contact in face gear drives by application of involute pinion. Avoidance of edge contact requires the changing of the shape of the pinion profiles.

Fig. 26 illustrates the variation of bending and contact stresses of the gear and the pinion during the cycle of meshing. The stresses are represented as functions of unitless parameter  $\phi$  represented as

$$\phi = \frac{\phi_P - \phi_{in}}{\phi_{fin} - \phi_{in}}, \quad 0 \leq \phi \leq 1 \quad (31)$$

Here:  $\phi_P$  is the pinion rotation angle,  $\phi_{in}$  and  $\phi_{fin}$  are the magnitudes of the pinion angular positions in the beginning and end of cycle of meshing.

The unitless stress coefficient  $\sigma$  (Fig. 26) is defined as

$$\sigma = \frac{\sigma_P}{\sigma_{P_{max}}}, \quad |\sigma| \leq 1 \quad (32)$$

Here:  $\phi_P$  is the variable of function of stresses and  $\phi_{P_{max}}$  is the magnitude of maximal stress. The increase of contact stresses during the cycle of meshing is caused by the edge contact.

## 5. Conclusions

Based on the research performed, the following conclusions may be drawn:

- (1) An analytical approach for determination of the worm thread surface, avoidance of singularities and worm dressing have been proposed.
- (2) Computer programs for generation of face gears by application of grinding or cutting worms have been developed. These computer programs cover also tooth contact analysis and stress analysis of face gear drives.
- (3) Automatization of the development of finite element models is proposed and the most time-consuming step in application of finite element analysis, the design of contacting models by using CAD computer programs, is avoided.
- (4) Generation of face gears by a shaper or grinding worm with rounded top edge is proposed to reduce bending stresses. Computations confirm that the bending stress can be reduced approximately 10%.

## References

- [1] Argyris, J., Litvin, F. L., Lian, Q., and Lagutin, S. A., *Determination of Envelope to Family of Planar Parametric Curves and Envelope Singularities*, Journal Computer Methods in Applied Mechanics and Engineering, Vol. 175, No. 1-2, pp. 175-187, 1999.
- [2] Argyris, J., Litvin, F.L., Peng, A., and Stadtfeld, H.J., *Axes of Meshing and Their Application in Theory of Gearing*, Journal Computer Methods in Applied Mechanics and Engineering, Vol. 163, No. 1-4, pp. 293-310, 1998.
- [3] Baumann, V., Bär, G., Haase, A., Hutschenreiter, B., Hünecke, C., and Dutschk, R., *BECAL 2.0 Programm zur Berechnung der Zahnflanken und Zahnfußbeanspruchung an Kegelrad- und Hypoidgetrieben bei Berücksichtigung der Verformungen und Abweichungen der Getriebe-elemente*, FVA-Heft 548, Forschungsvereinigung Antriebstechnik, 1998.
- [4] Bär, G., *Curvatures of the Enveloped Helicoid*, Mechanism and Machine Theory, Vol. 32, No. 1, pp. 111-120, 1997.
- [5] Hibbit, Karlsson & Sirensen, Inc., *ABAQUS/Standard 6.1 User's Manual*, 1800 Main Street, Pantucket, RI 02860-4847, 1998.
- [6] Korn, G. A. and Korn, T. M., *Mathematics Handbook for Scientist and Engineers*, McGraw-Hill, Inc., 2nd Ed., 1968.
- [7] Litvin, F. L., *Theory of Gearing*, NASA RP-1212 (AVSCOM 88-C-C035), Washington, D. C., 1989.
- [8] Litvin, F. L., *Gear Geometry and Applied Theory*, Prentice Hall, Inc., Englewood Cliffs, New Jersey, 1994.
- [9] Litvin, F. L., *Development of Gear Technology and Theory of Gearing*, NASA Reference Publication 1406, ARL-TR-1500, 1998.
- [10] Litvin, F. L., Demenego, A., and Vecchiato, D., *Formation by Branches of Envelope to Parametric Families of Surfaces and Curves*, Journal Computer Methods in Mechanics and Engineering, Vol. 190, pp. 4587-4608, 2001.
- [11] Litvin, F. L., Egelja, A. M., and De Donno, M., *Computerized Determination of Singularities and Envelopes to Family of Contact Lines on Gear Tooth Surface*, Journal Computer Methods in Applied Mechanics and Engineering, Vol. 158, No. 1-2, pp. 23-34, 1998.
- [12] Litvin, F. L., De Donno, M., Peng, A., Vorontsov, A., and Handschuh, R. F., *Integrated Computer Program for Simulation of Meshing and Contact of Gear Drives*, Computer Methods in Applied Mechanics and Engineering, Vol. 181, No. 1-3, pp. 71-85, 2000.
- [13] Litvin, F. L., Peng, A., and Wang, A. G., *Limitation of Gear Tooth Surfaces by Envelopes to Contact Lines and Edge of Regression*, Mechanism and Machine Theory, Vol. 34, No. 6, pp. 889-902, 1999.
- [14] Litvin, F. L., Chen, Y.-J., Heath, G. F., Sheth, V. J., Chen, N., *Apparatus and Method for Precision Grinding Face Gears*, USA Patent 6,146,253, 2000.
- [15] Miller, E. W., *Hob for Generation Crown Gears*, USA Patent 2,304,588, 1942.
- [16] Sheveleva, G. I., *Mathematical simulation of spiral bevel gear production and meshing processes with contact and bending stresses*, In Proc. IX World Congr. IFTOMM, Vol. 1, pp. 509-513, 1995.
- [17] Stadtfeld, H. J., *Handbook of Bevel and Hypoid Gears: Calculation, Manufacturing, and Optimization*, Rochester Institute of Technology, Rochester, New York, 1993.

- [18] Stosic, N., *On Gearing of Helical Screw Compressor Rotors*, Proc IMechE, Journal of Mechanical Engineering Science, Vol. 212, pp. 587-594, 1998.
- [19] Stosic, N., *Recent developments in screw compressors*, Proc IMechE, Journal of Mechanical Engineering Science, C542/066, 1999.
- [20] Stosic, N. and Hanjalic, K., *Development and Optimization of Screw Machines With a Simulation Model. Part I: Profile generation*, ASME Transactions, Journal of Fluids Engineering, Vol. 119, pp. 659-663, 1997.
- [21] Zalgaller, V. A., *Theory of Envelopes*, Publishing House Nauka (in Russian), 1975.
- [22] Zalgaller, V. A. and Litvin, F. L., *Sufficient Condition of Existence of Envelope to Contact Lines and Edge of Regression on the Surface of the Envelope to the Parametric Family of Surfaces represented in Parametric Form*, Proceedings of Universities: Mathematics (in Russian), Vol. 178, No. 3, pp. 20-23, 1977.
- [23] Zienkiewicz, O. C. and Taylor, R. L., *The Finite Element Method*, John Wiley & Sons, 5th Ed., 2000.

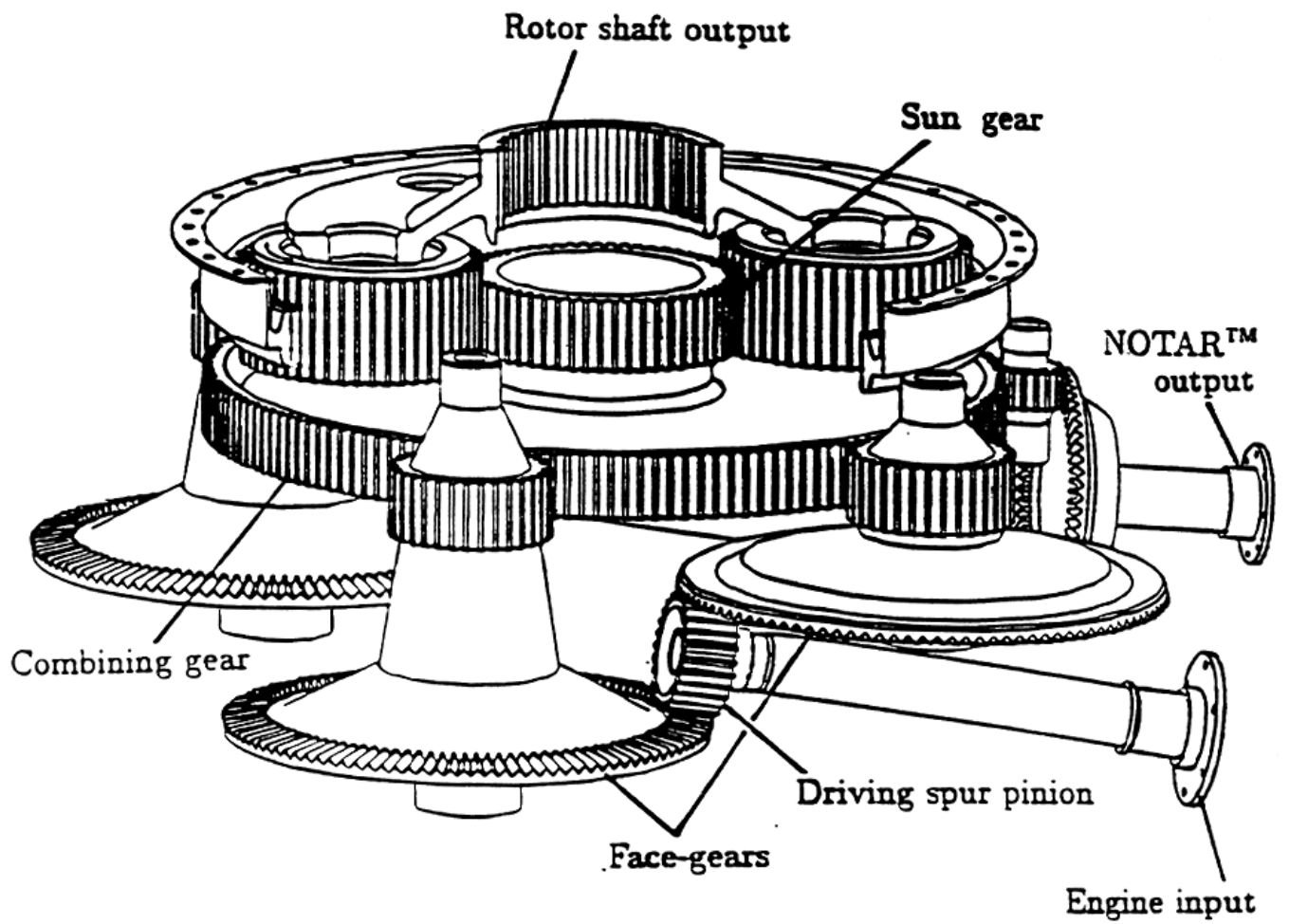


Figure 1: Application of face gear drive in helicopter transmission

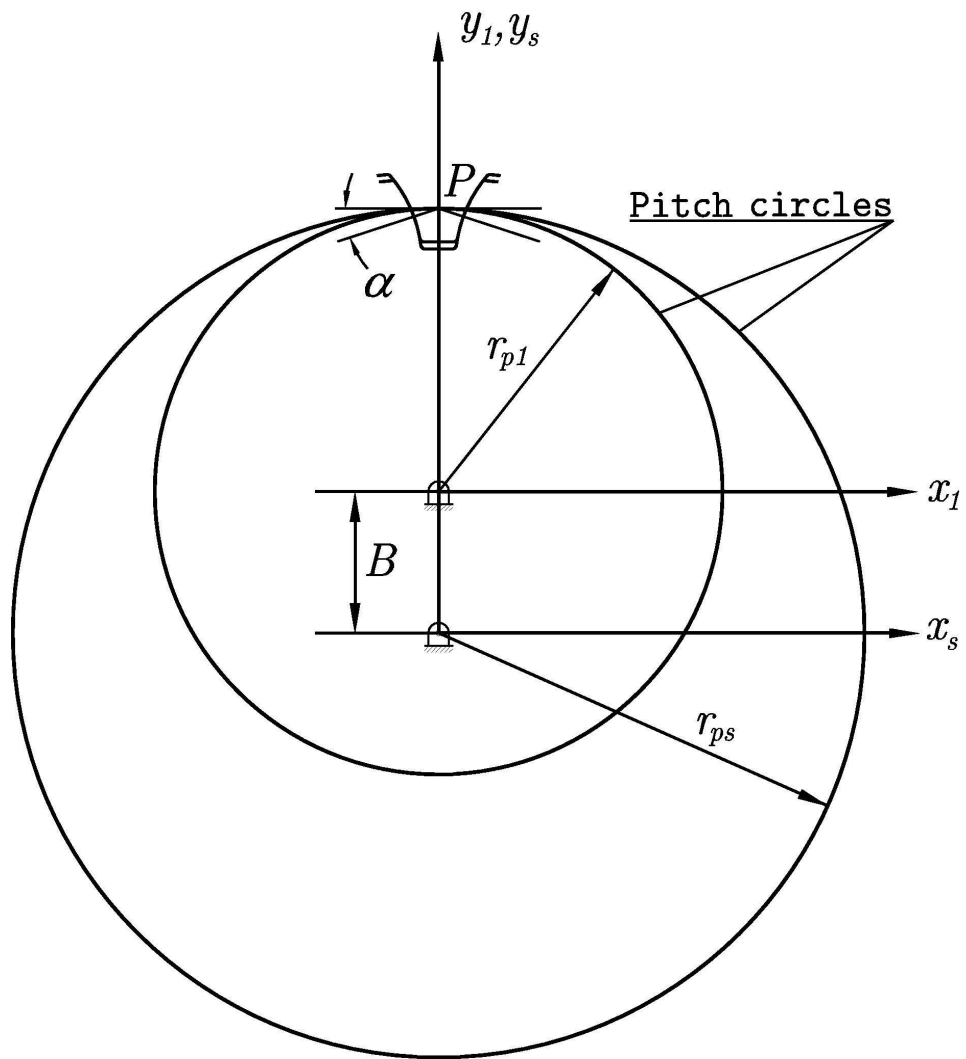
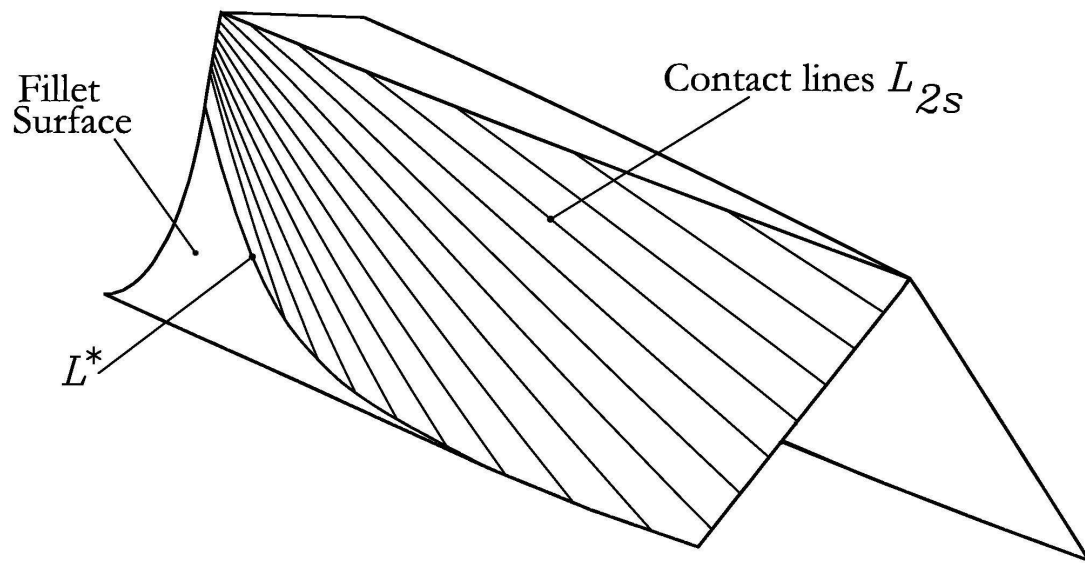
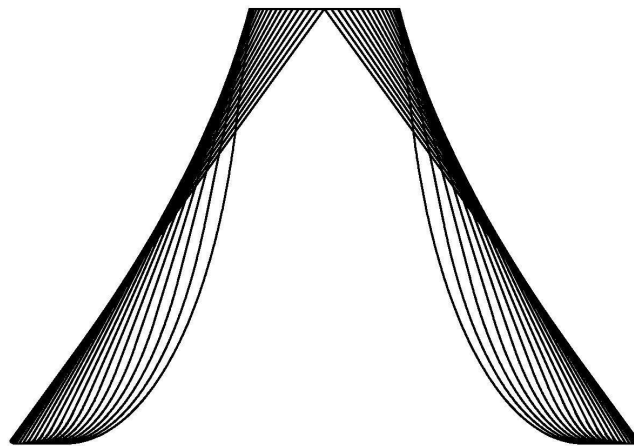


Figure 2: Pitch circles and tooth profiles of pinion and shaper



(a)



(b)

Figure 3: Structure of face-gear tooth: (a) lines contact  $L_{2s}$  and fillet; (b) cross-section of face-gear tooth

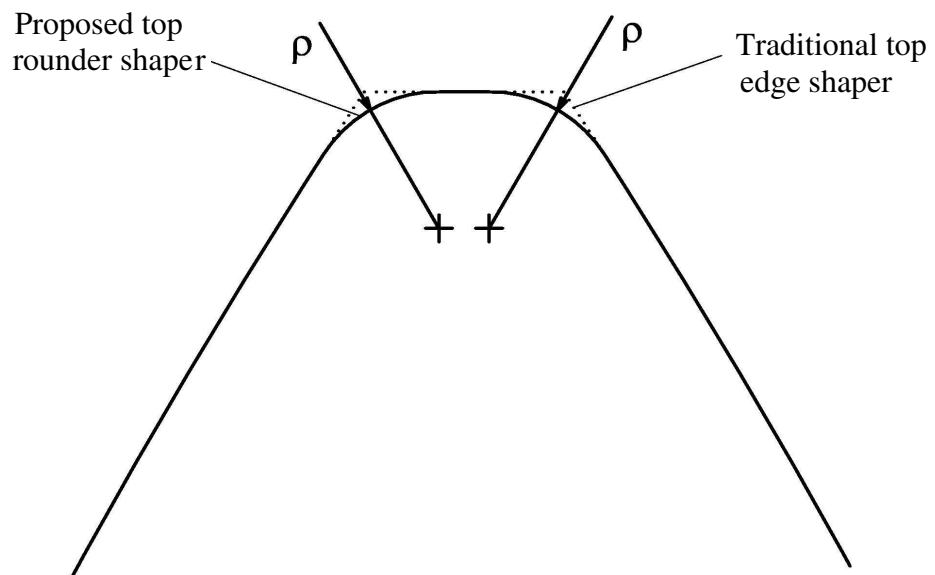
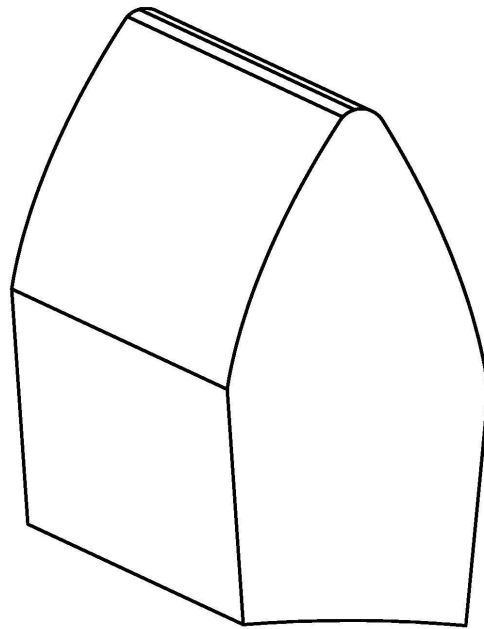


Figure 4: Shaper with a rounded edge

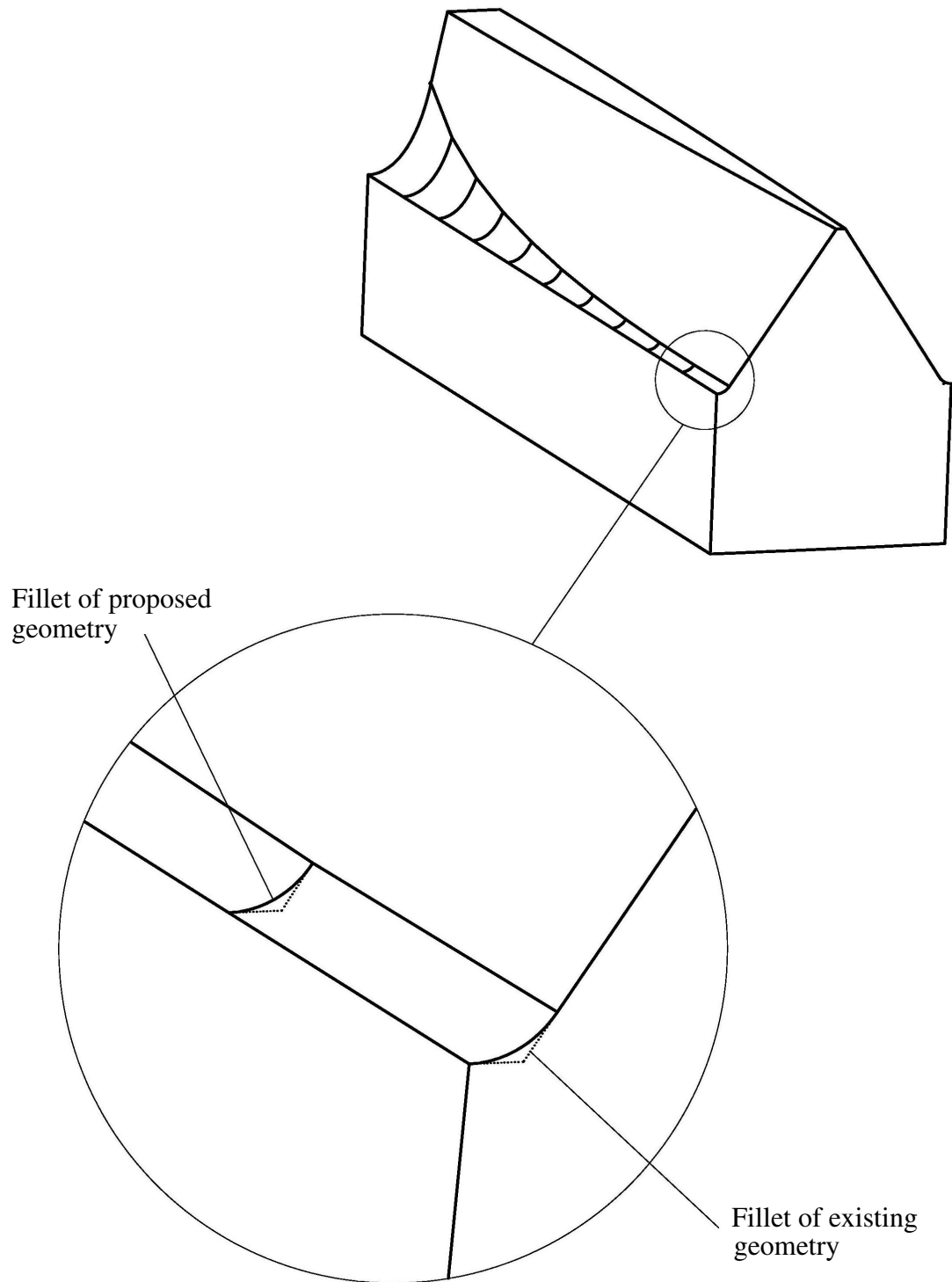


Figure 5: Shape of the modified fillet of the face-gear

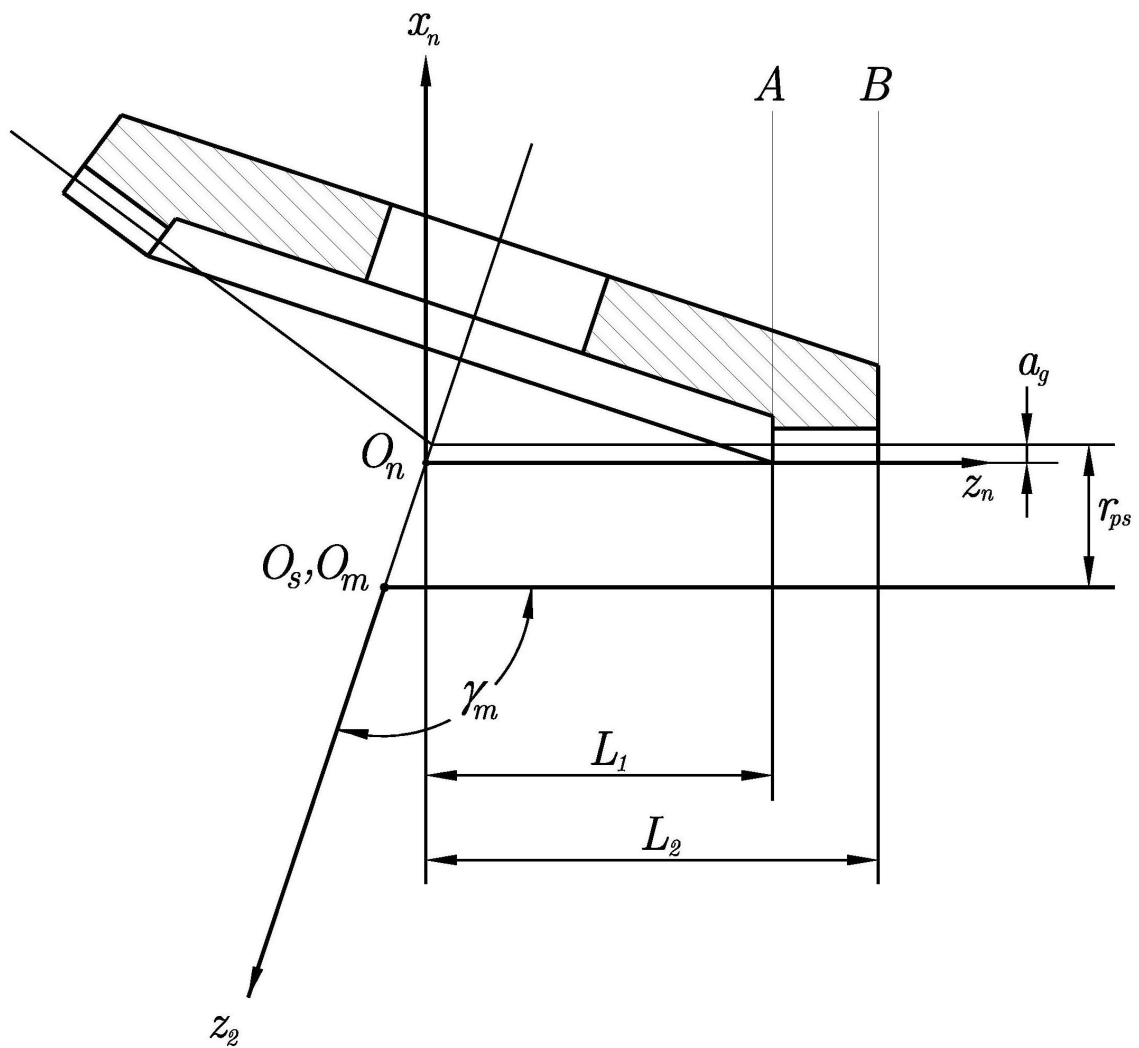


Figure 6: Limitation of length of tooth of face-gear

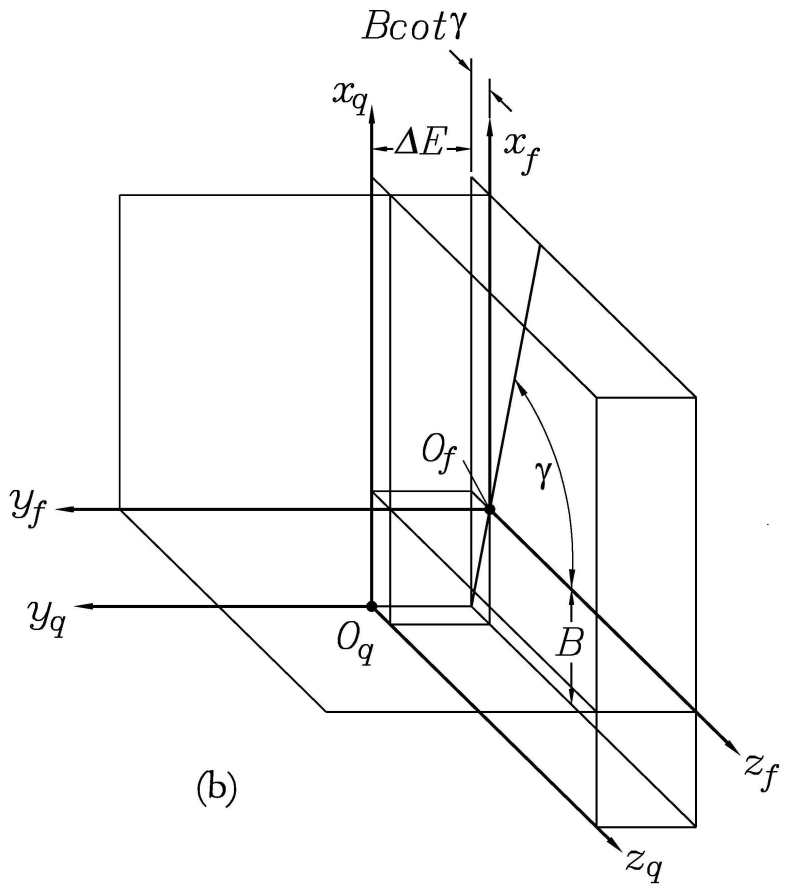
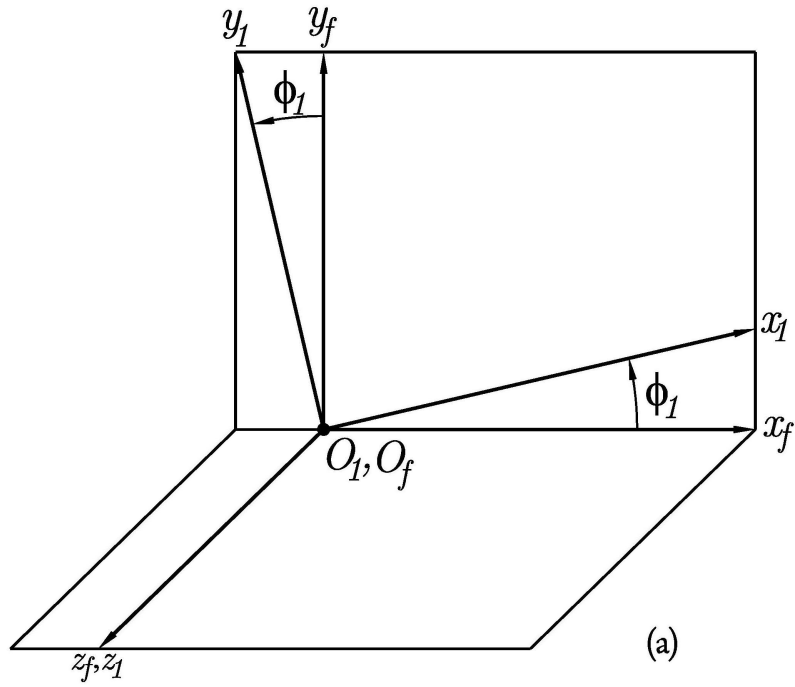


Figure 7: Coordinate systems applied for simulation of meshing: (a) coordinate systems  $S_1$  and  $S_f$ ; (b) coordinate systems  $S_f$  and  $S_q$

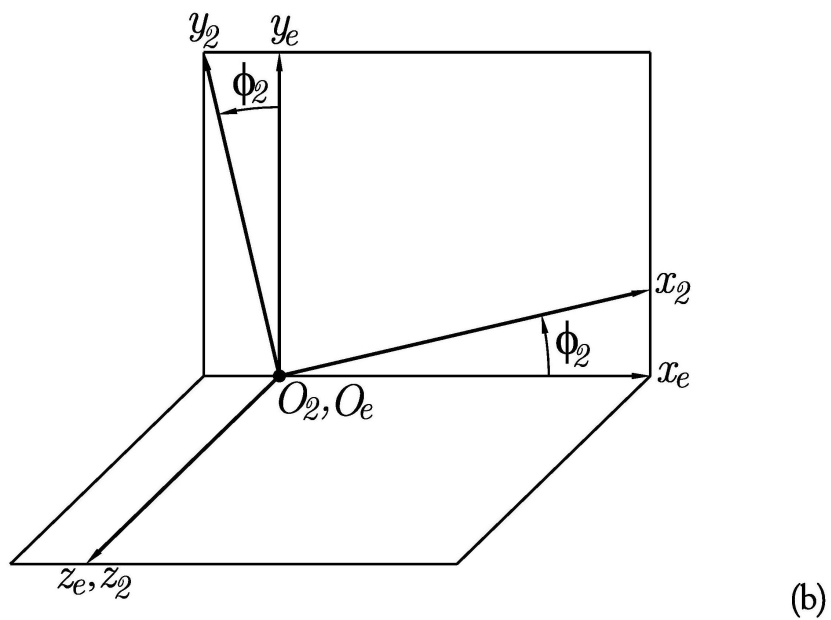
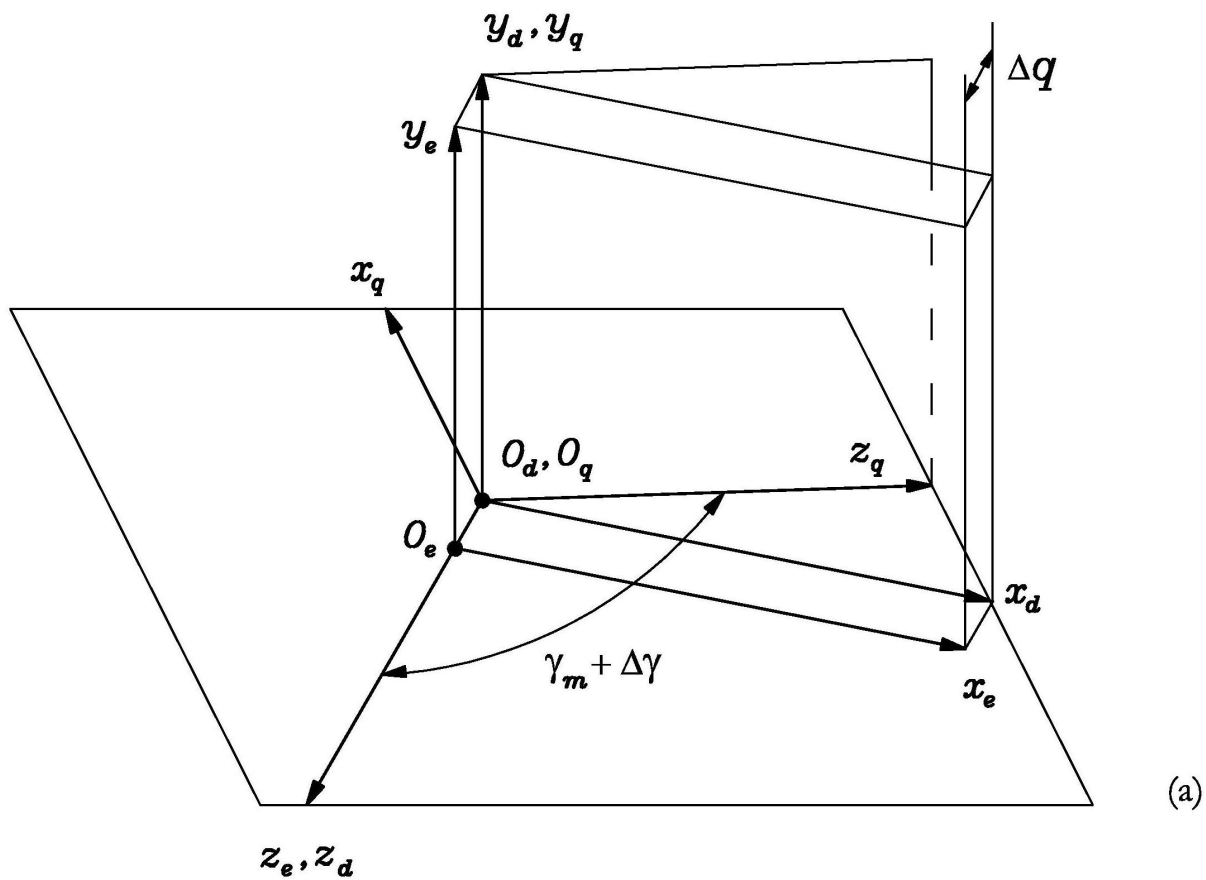
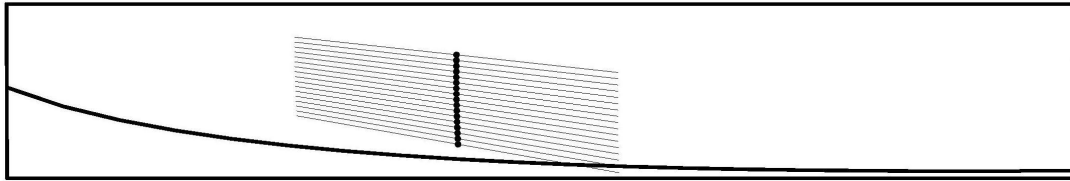
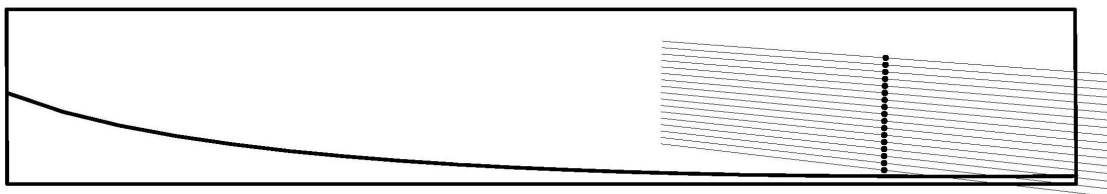


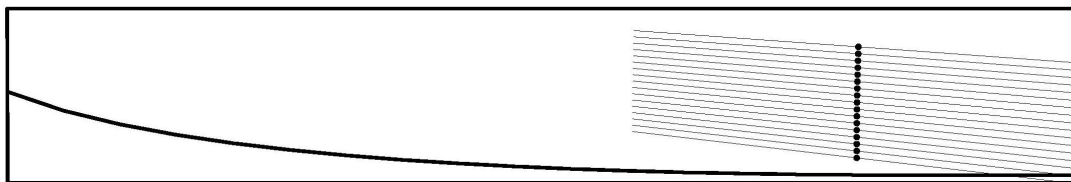
Figure 8: Coordinate systems applied for simulation of meshing: (a) coordinate systems  $S_q, S_d, S_e$ ; (b) coordinate systems  $S_2, S_e$



(a)

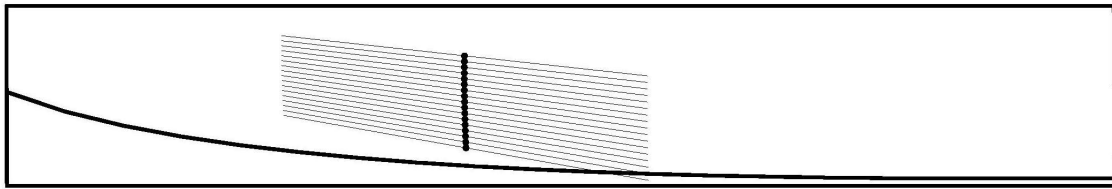


(b)

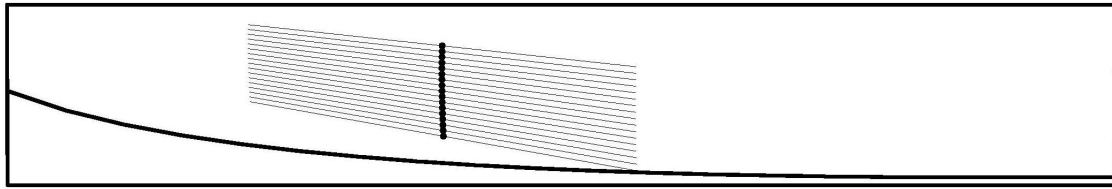


(c)

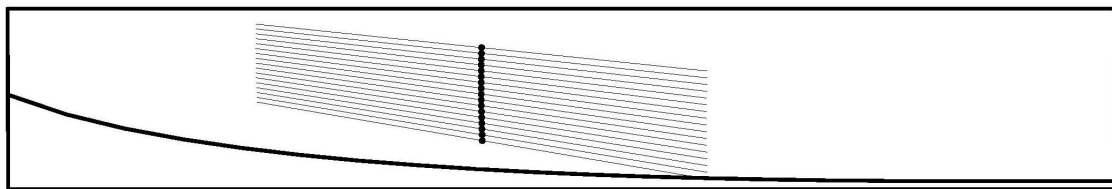
Figure 9: Path of contact and bearing contact for the following examples: (a) No errors of alignment; (b)  $|\Delta\gamma| = 3 \text{ arcmin}$ ; (c)  $|\Delta E| = 1000 \mu m$



(a)



(b)



(c)

Figure 10: Adjustment of path of contact by applying the axial displacement  $\Delta q$  of the face gear with respect to the pinion: (a)  $|\Delta\gamma| = 3 \text{ arcmin}$ ,  $|\Delta q| = 550 \mu\text{m}$ ; (b)  $|\Delta E| = 1000 \mu\text{m}$ ,  $|\Delta q| = 500 \mu\text{m}$ ; (c)  $|\Delta\gamma| = 3 \text{ arcmin}$ ,  $|\Delta E| = 1000 \mu\text{m}$ ,  $|\Delta q| = 1000 \mu\text{m}$

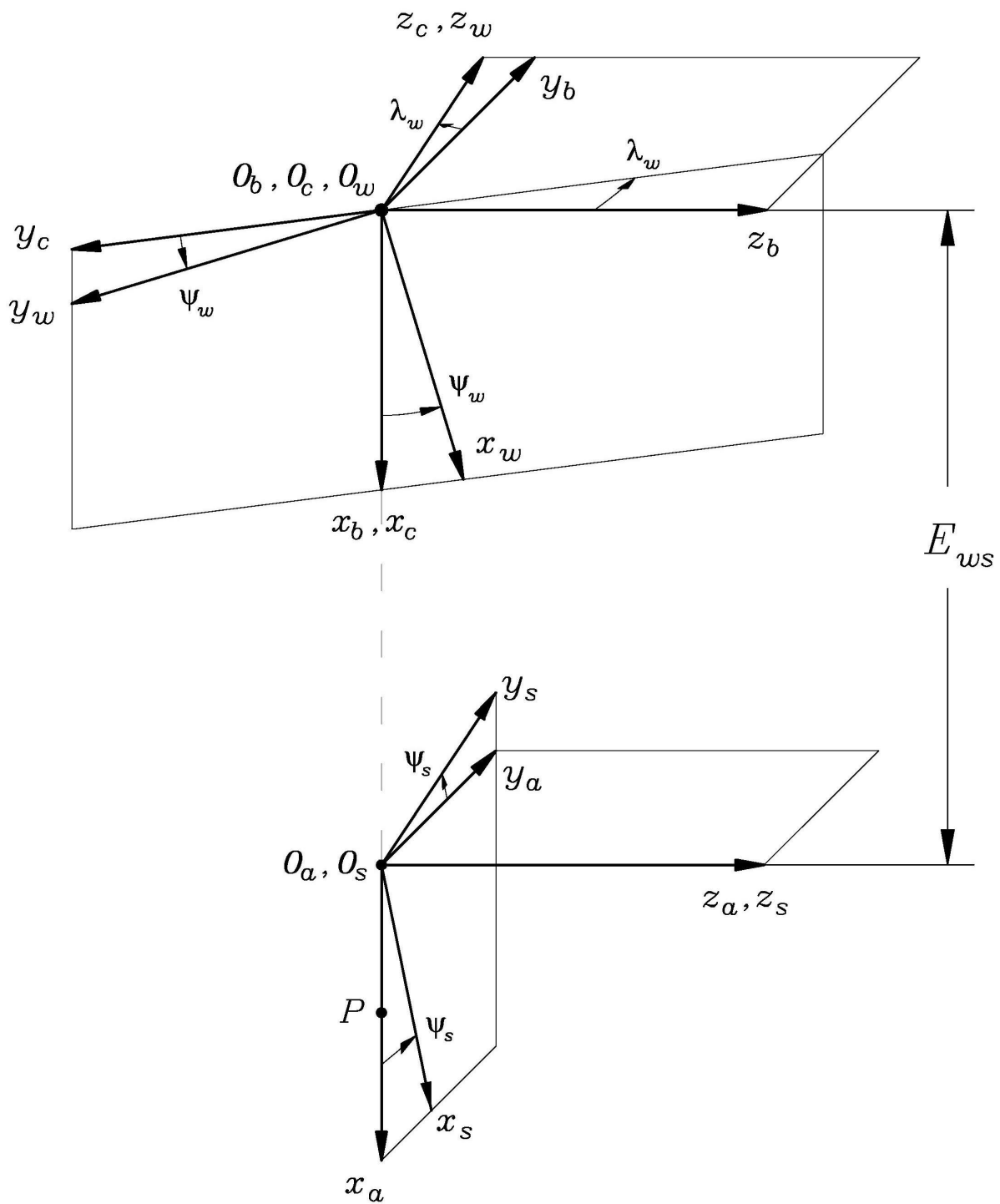


Figure 11: Coordinate systems  $S_s$  and  $S_w$  and worm installment

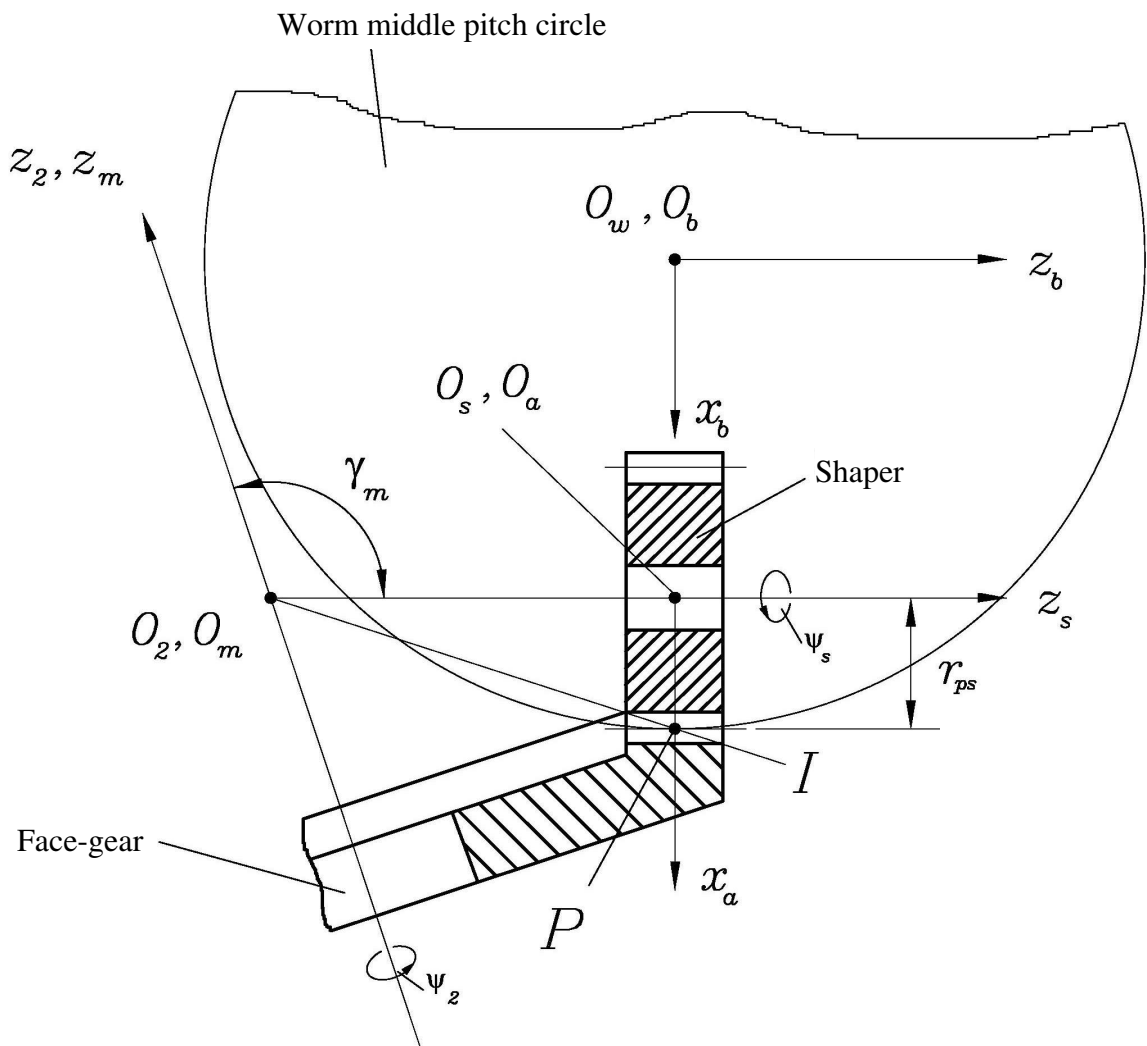


Figure 12: For derivation of tangency of surfaces  $\Sigma_s$  and  $\Sigma_2$  and generation of the face-gear by the worm

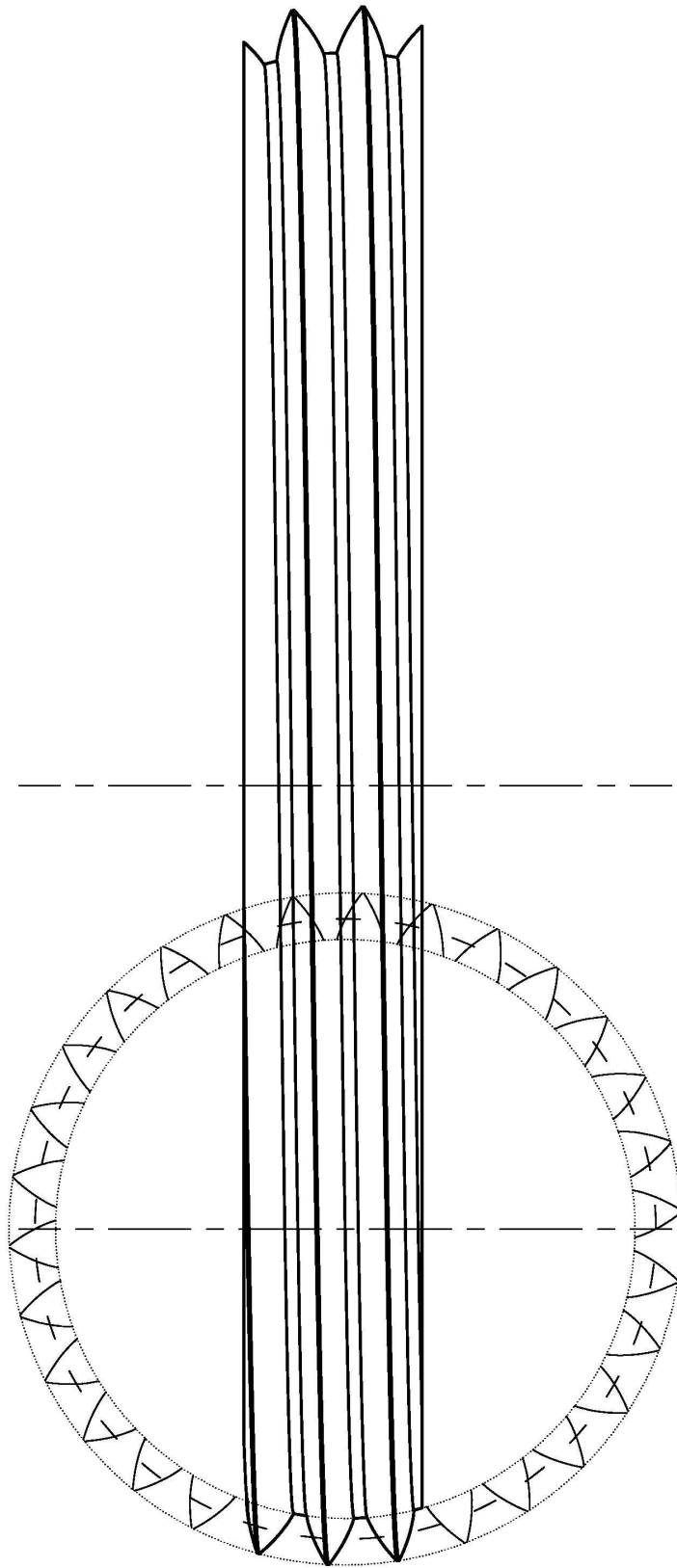


Figure 13: Schematic illustration of meshing of the shaper and the worm

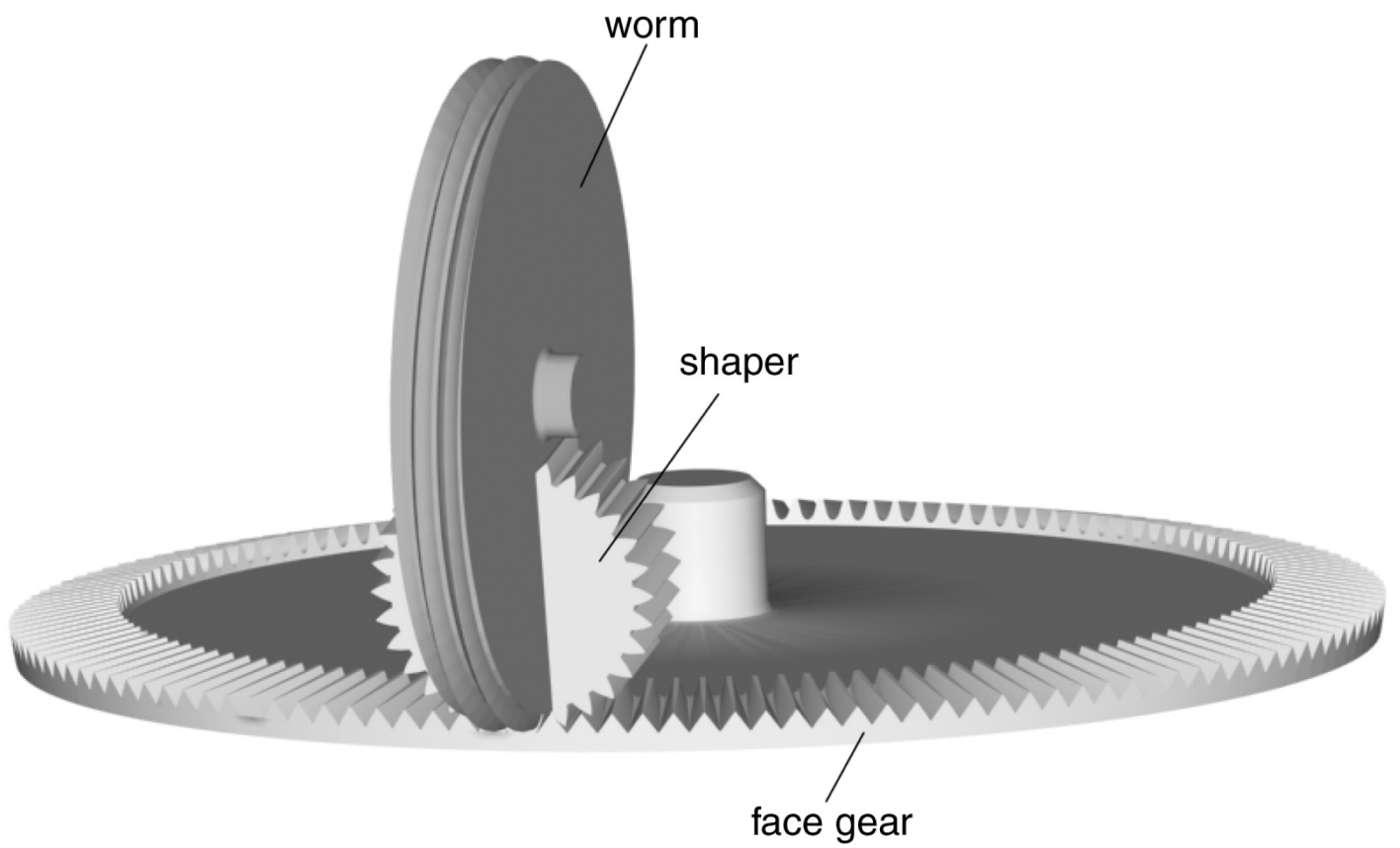


Figure 14: Illustration of simultaneous meshing of shaper, worm, and face-gear

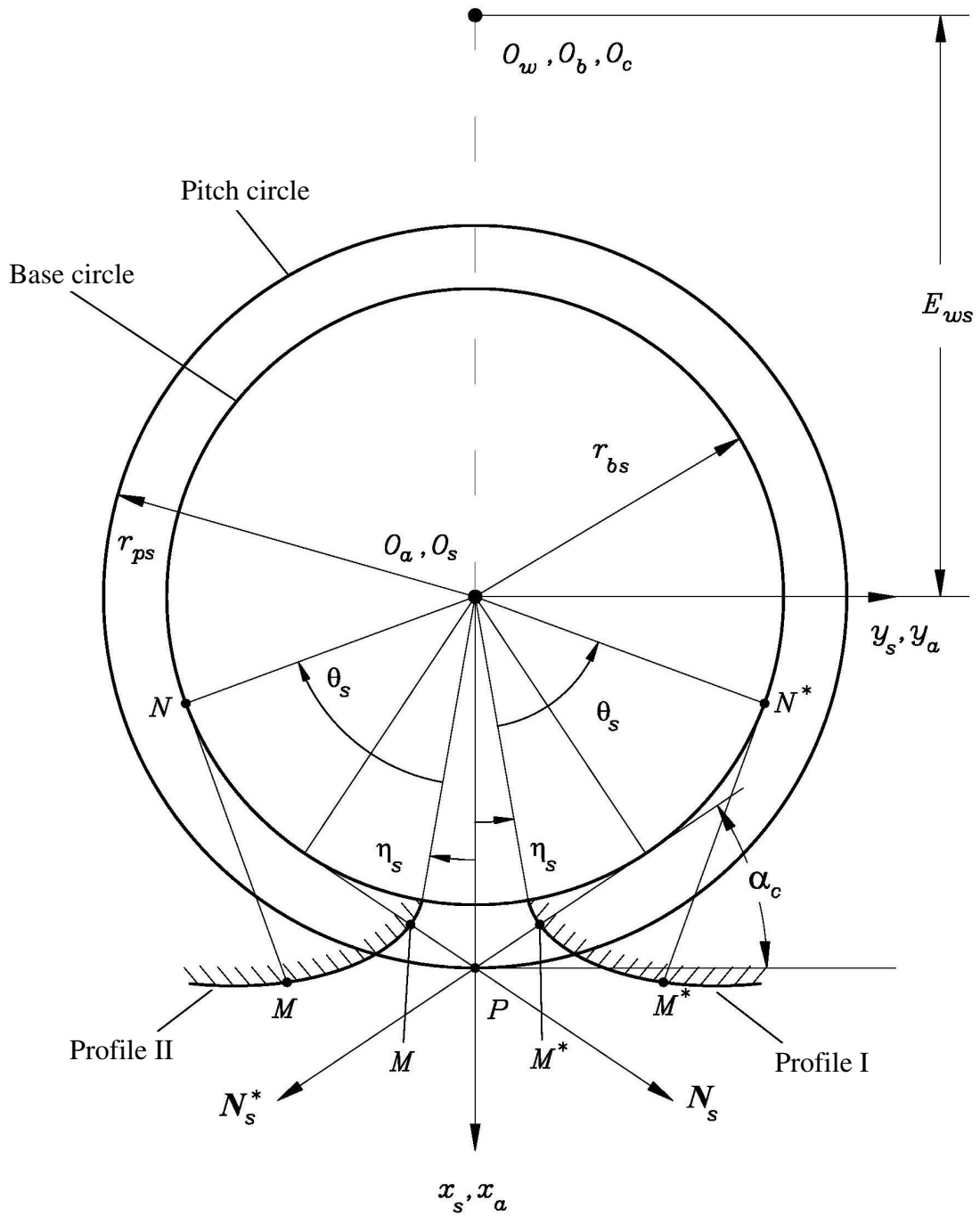


Figure 15: Shaper profiles and normals to shaper profiles

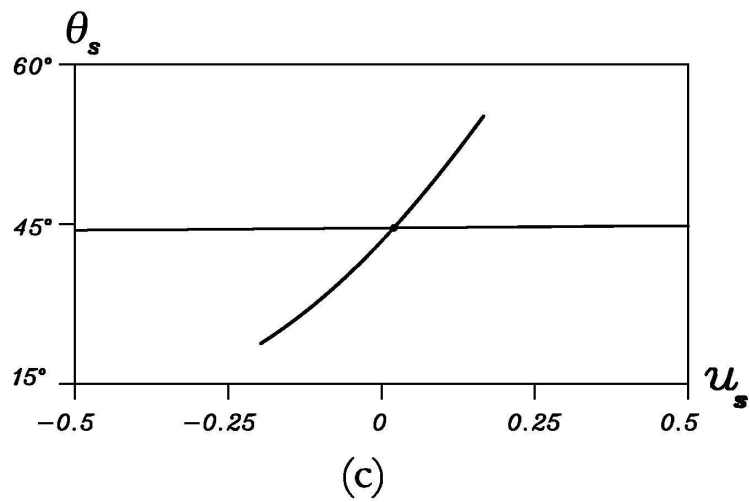
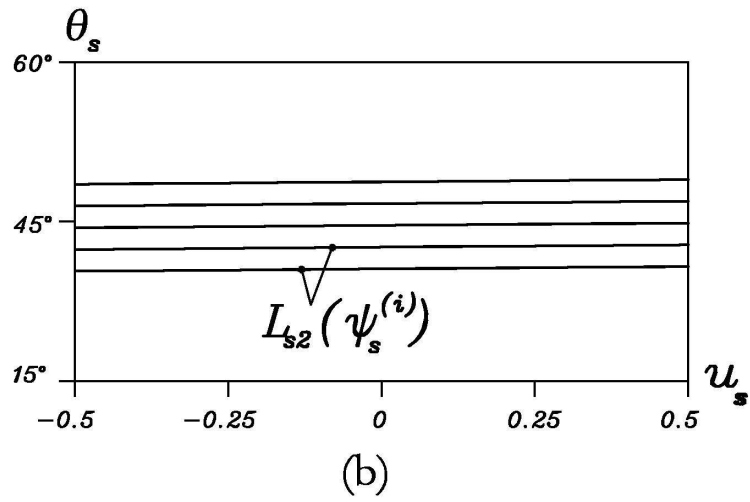
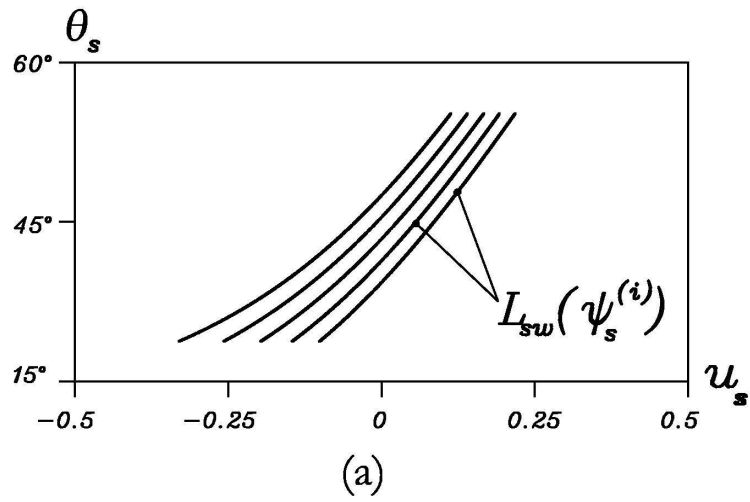


Figure 16: Illustration of lines of tangency (a) lines  $L_{sw}$  of tangency of  $\Sigma_s$  and  $\Sigma_w$ ; (b) lines  $L_{s2}$  of tangency of  $\Sigma_s$  and  $\Sigma_2$ , (c) intersection of  $L_{sw}$  and  $L_{s2}$

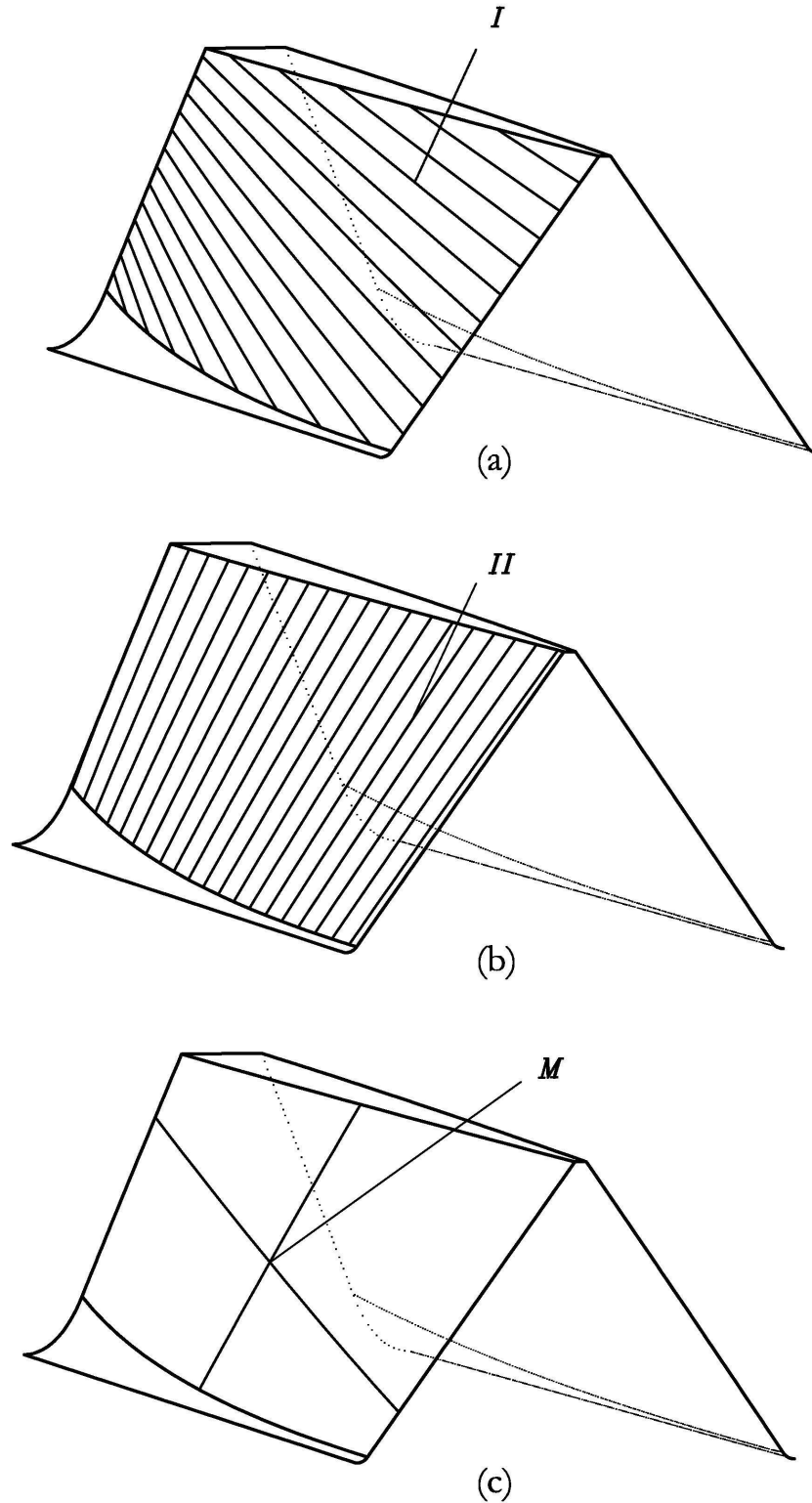


Figure 17: For illustration of meshing of surfaces  $\Sigma_2$  and  $\Sigma_w$ : (a) lines of tangency of  $\Sigma_2$  and  $\Sigma_w$  wherein  $\psi_w = \text{constant}$ , (b) lines of tangency of  $\Sigma_2$  and  $\Sigma_w$  wherein  $l_w = \text{constant}$  and (c) point  $M$  of tangency of  $\Sigma_2$  and  $\Sigma_w$

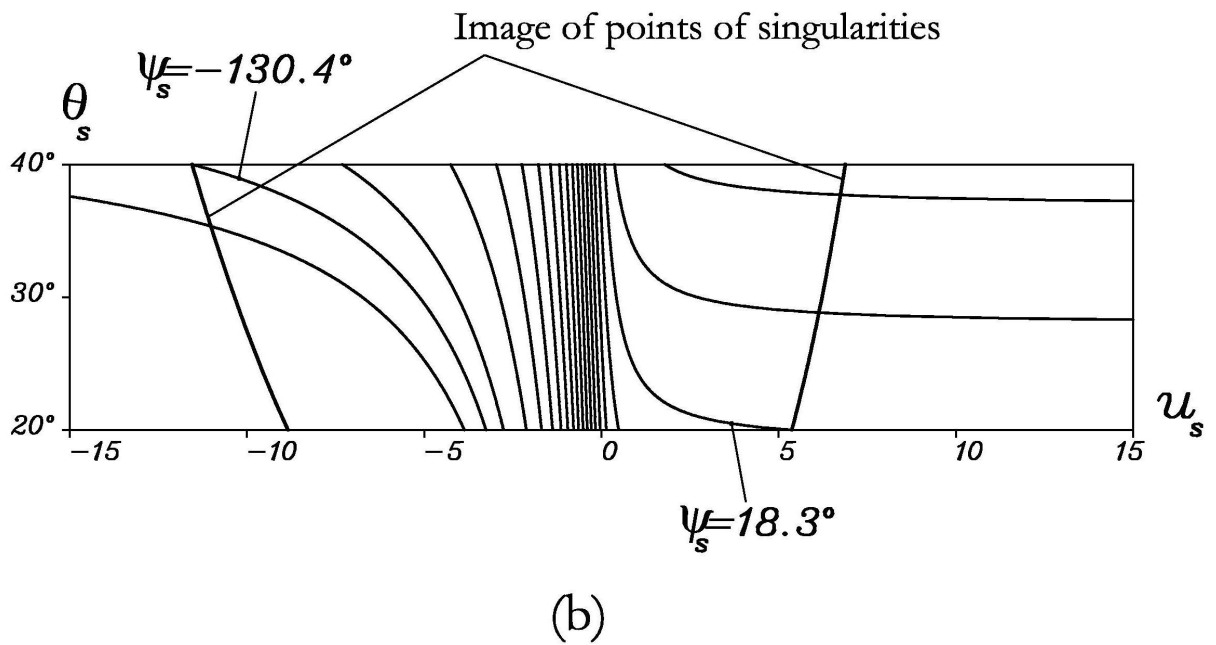
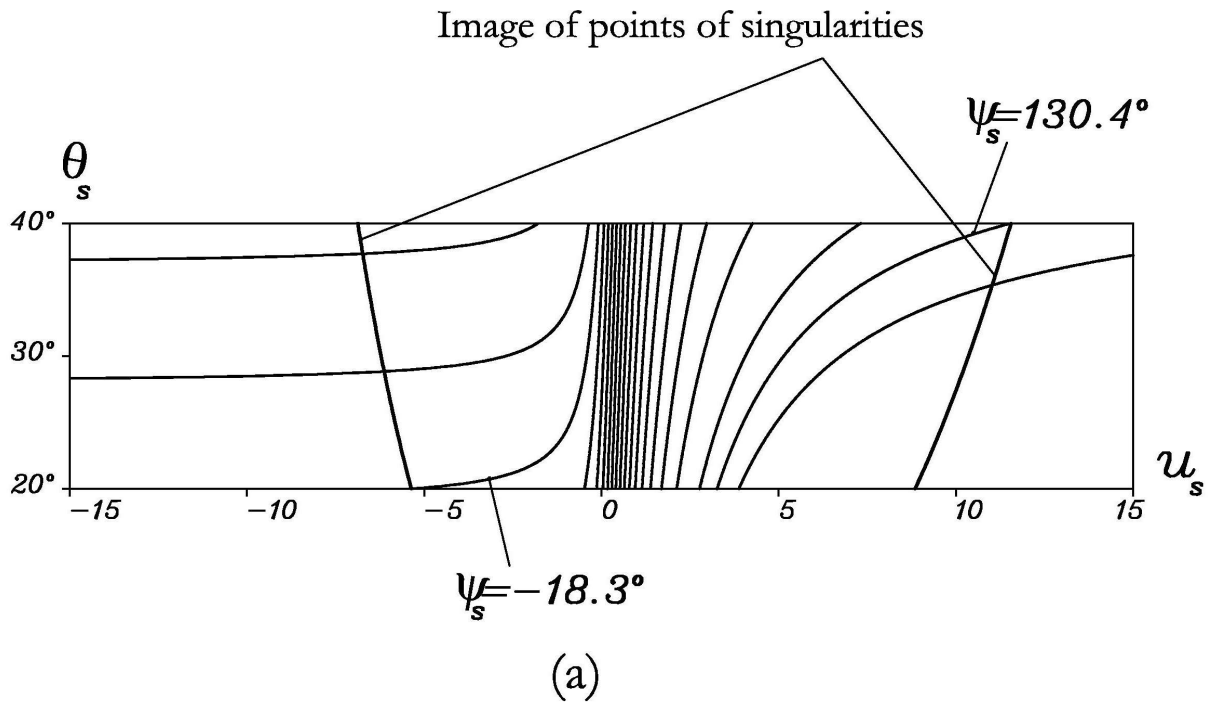


Figure 18: Contact lines between the shaper and the worm in plane  $(u_s, \theta_s)$ : (a) for surface shaper with profile I, and (b) profile II (see Fig. 14)

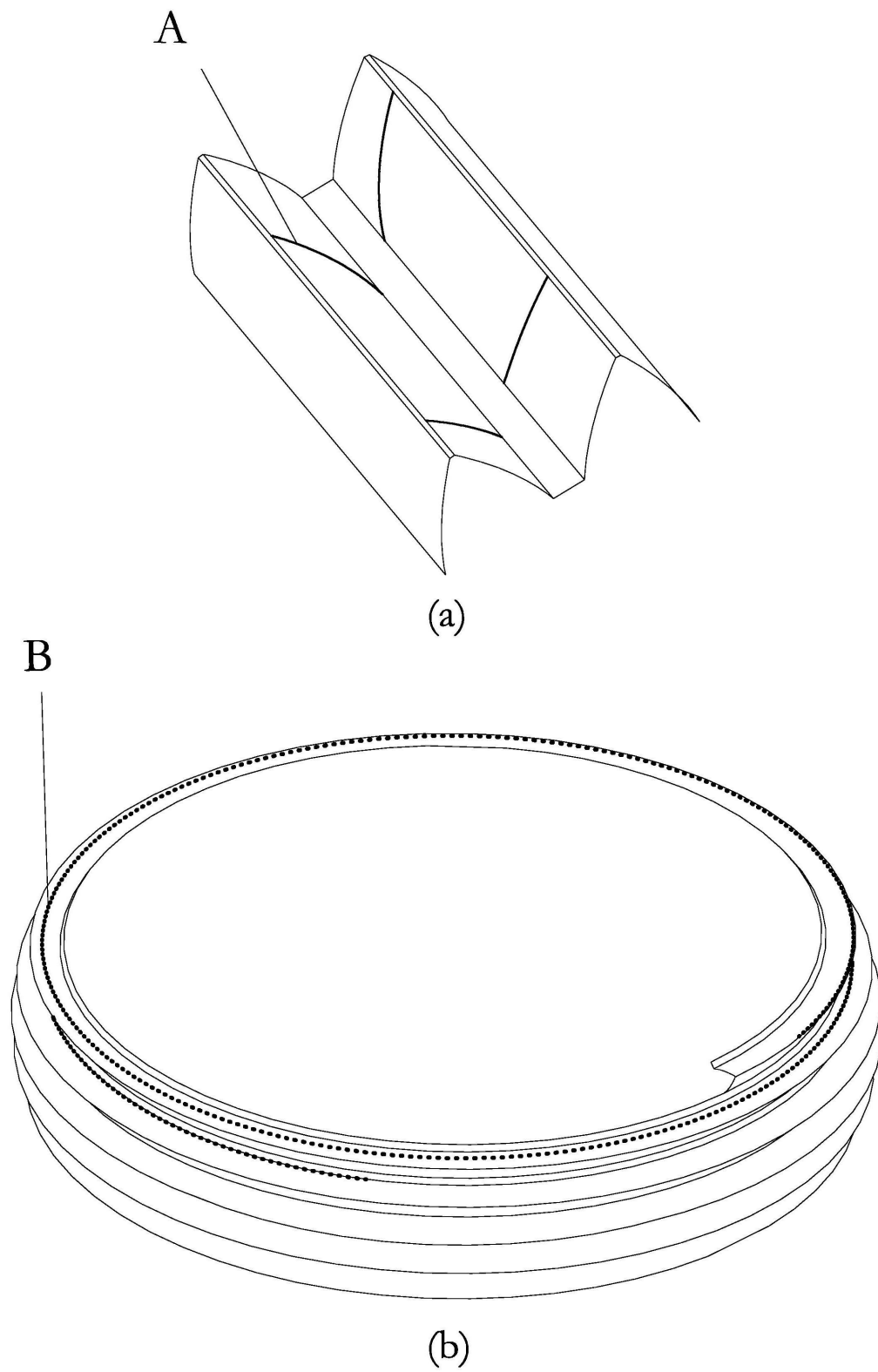


Figure 19: Illustration of worm singularities: (a) regular points A of shaper that generate worm singularities; (b) singularities B on worm threads surface

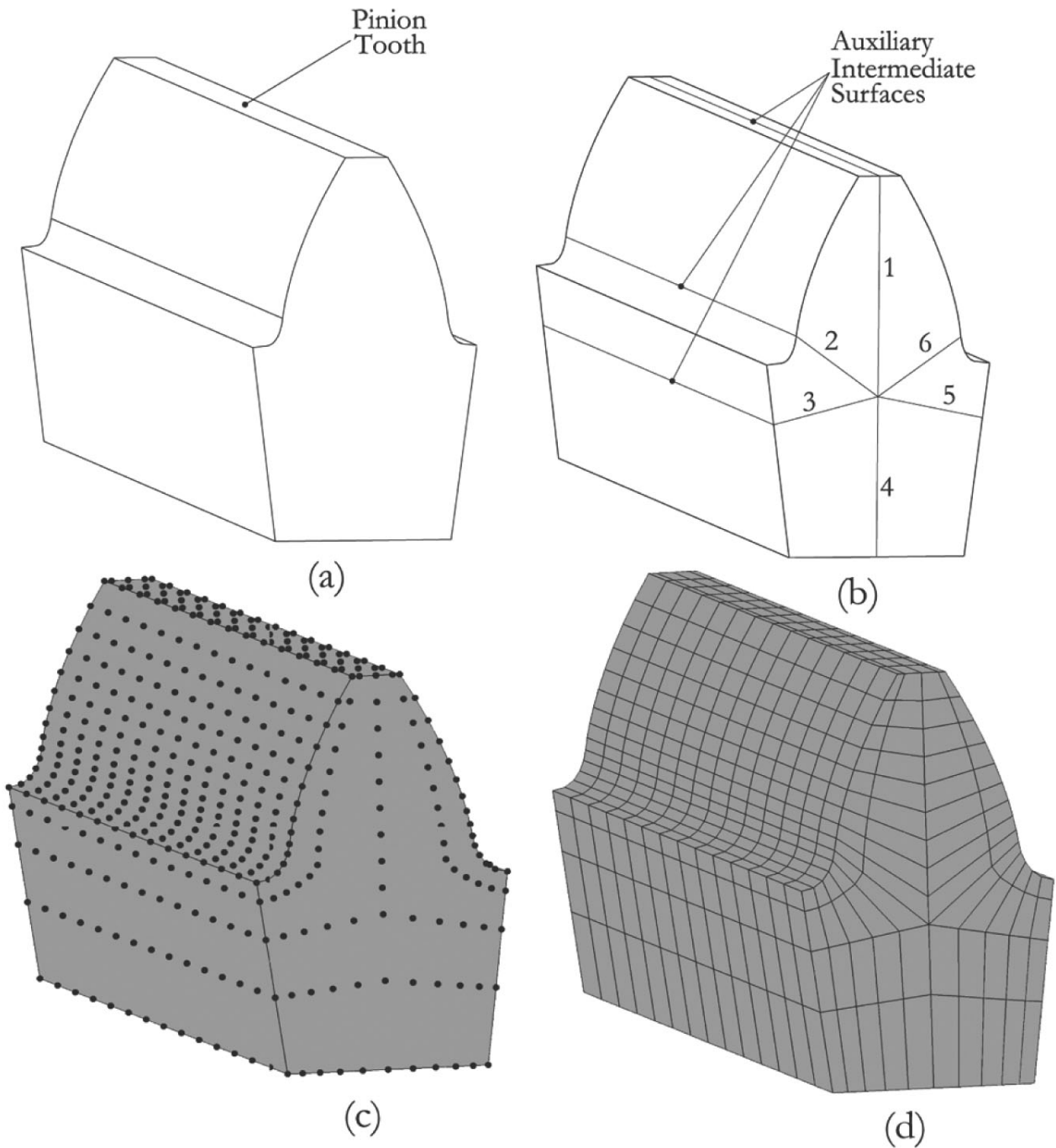


Figure 20: Illustrations of: (a) the volume of designed body, (b) auxiliary intermediate surfaces, (c) determination of nodes for the whole volume, and (d) discretization of the volume by finite elements

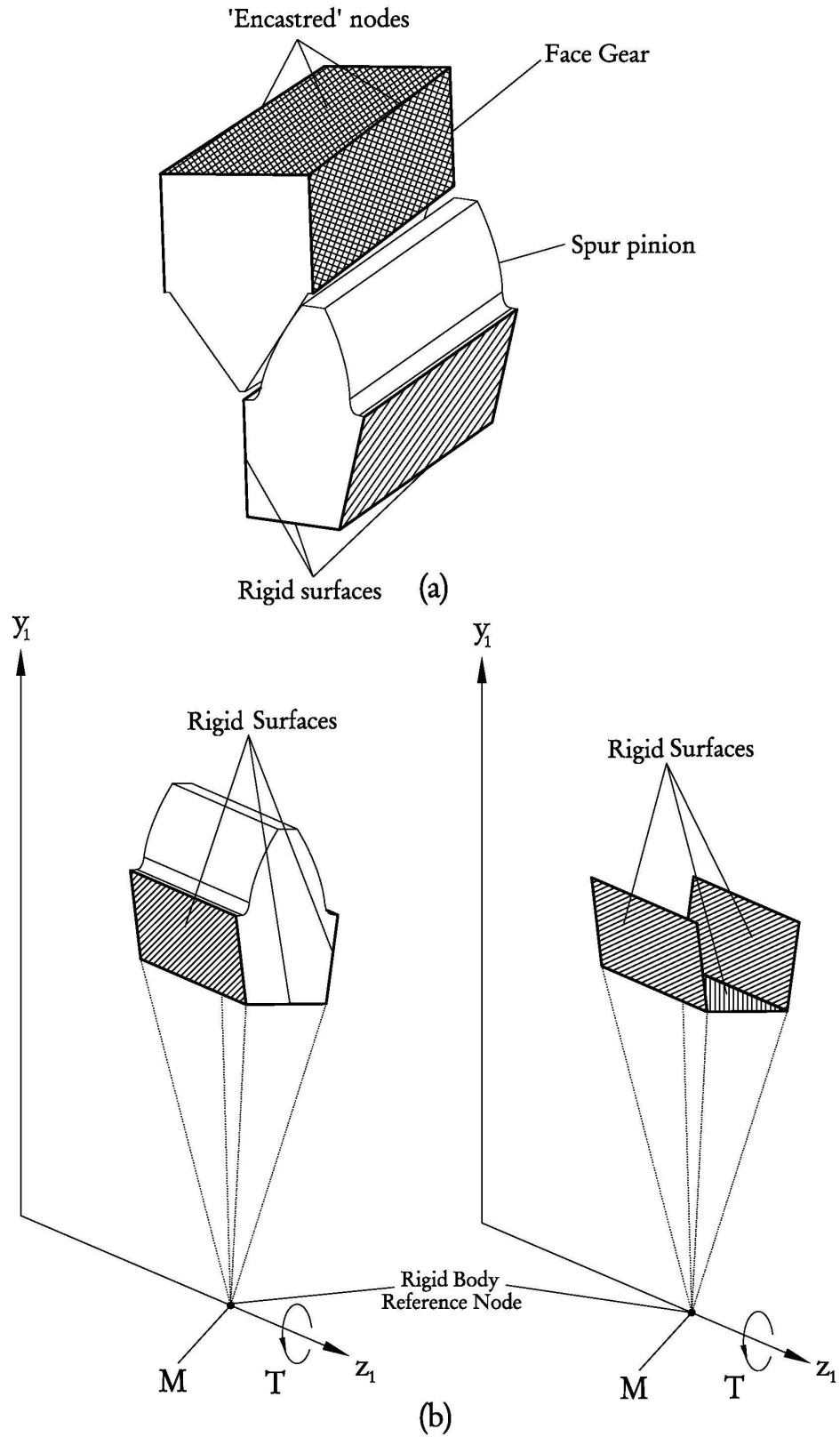


Figure 21: Schematic illustration of: (a) boundary conditions for the pinion and the face-gear, and (b) rigid surfaces applied for boundary conditions of the pinion

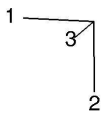
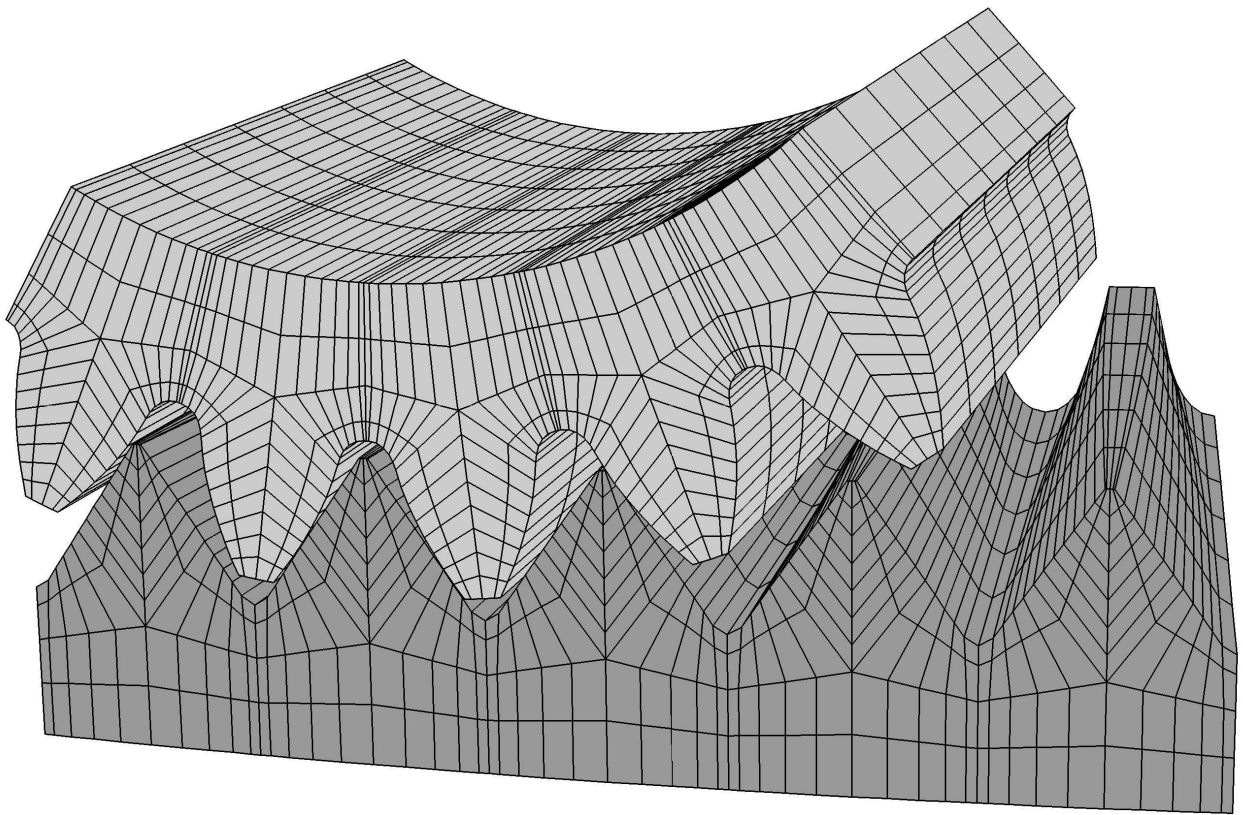


Figure 22: Five-pairs-of-teeth face-gear drive model

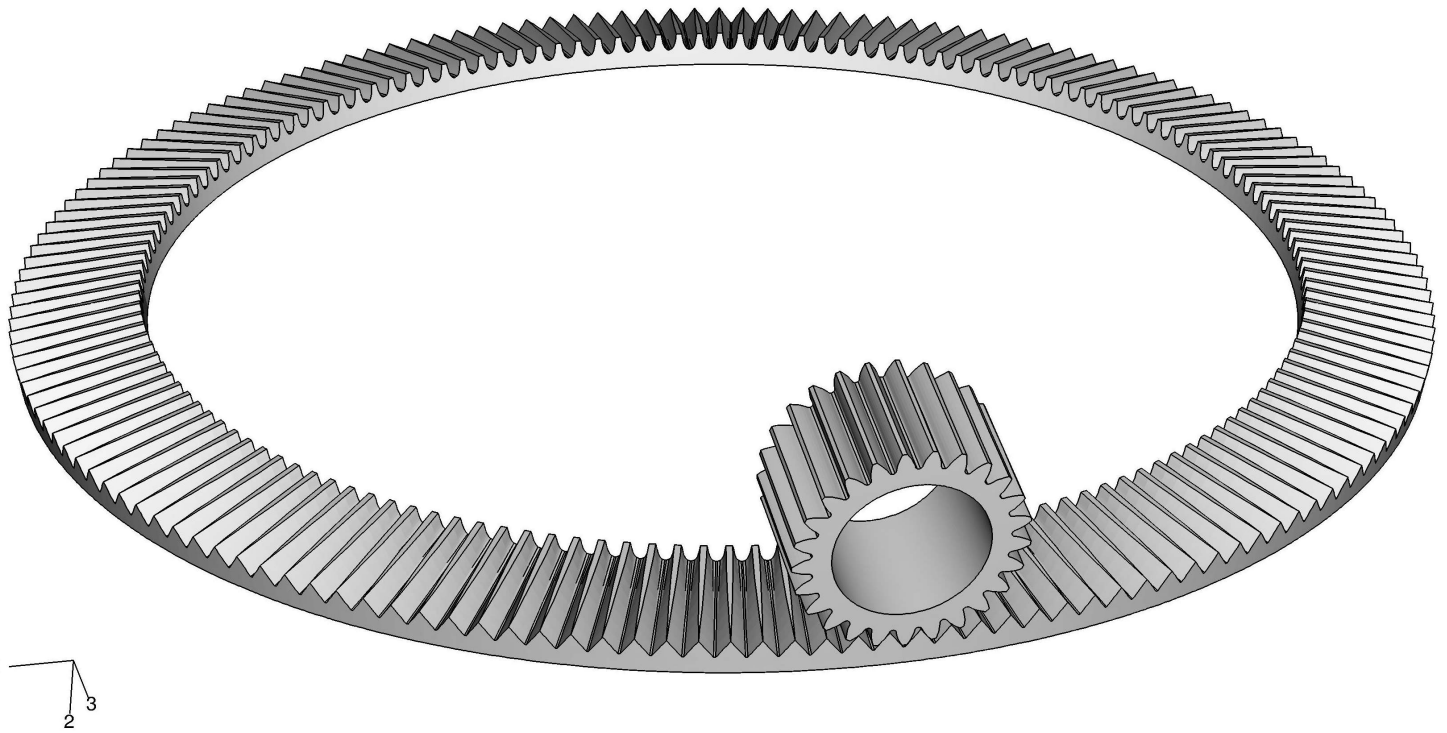


Figure 23: Whole gear drive model

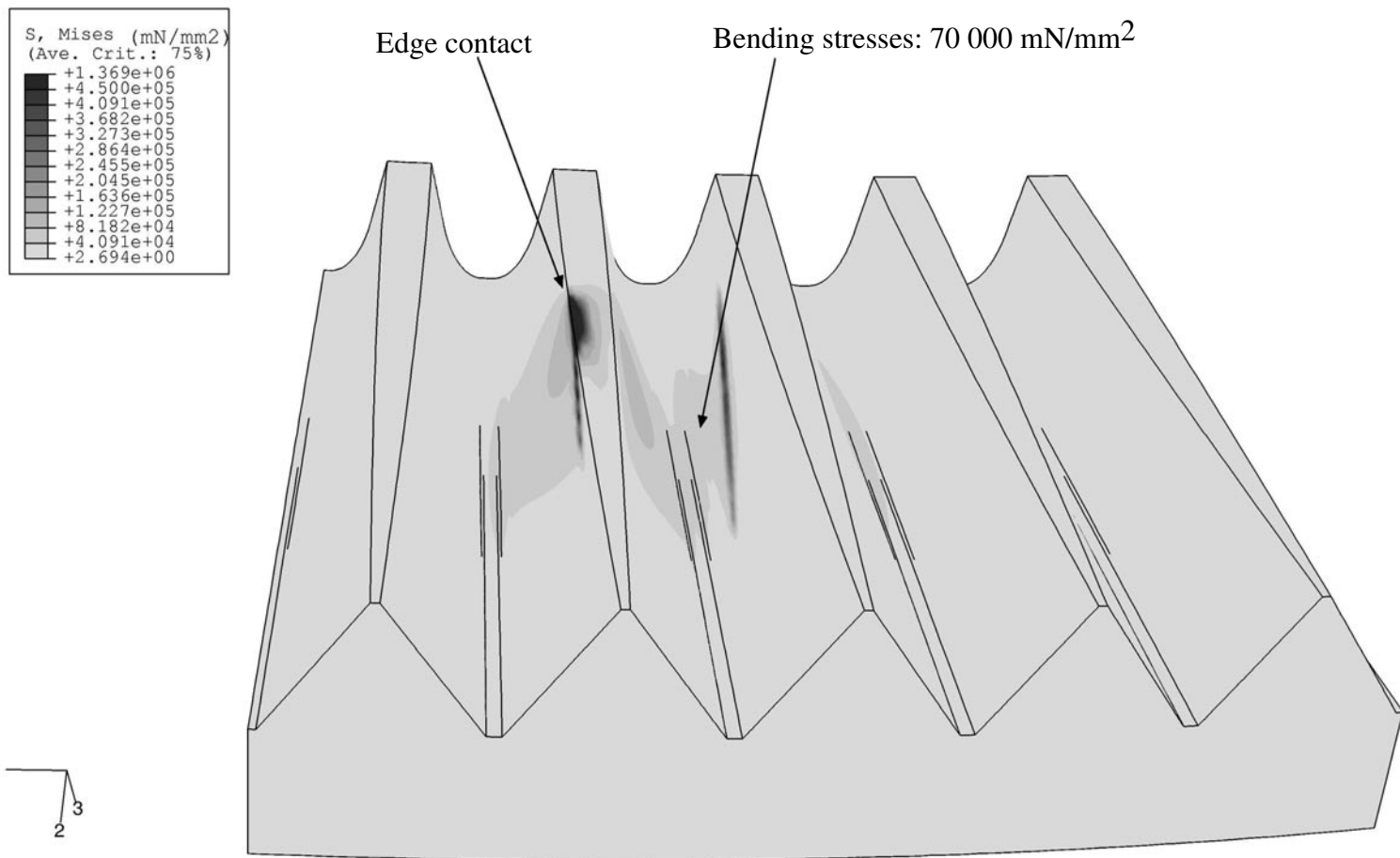


Figure 24: Contact and bending stresses for version 1 of face-gear drive

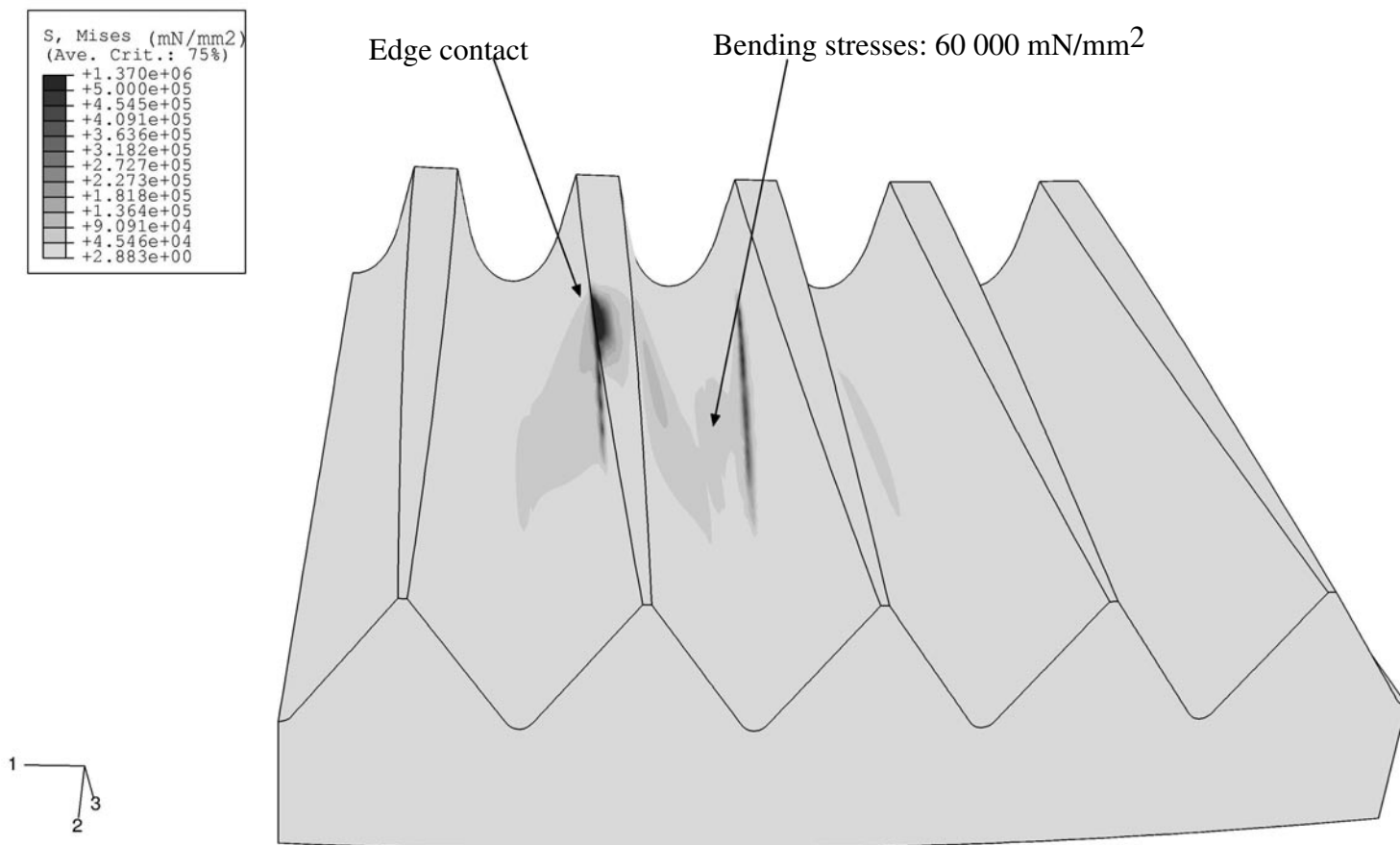
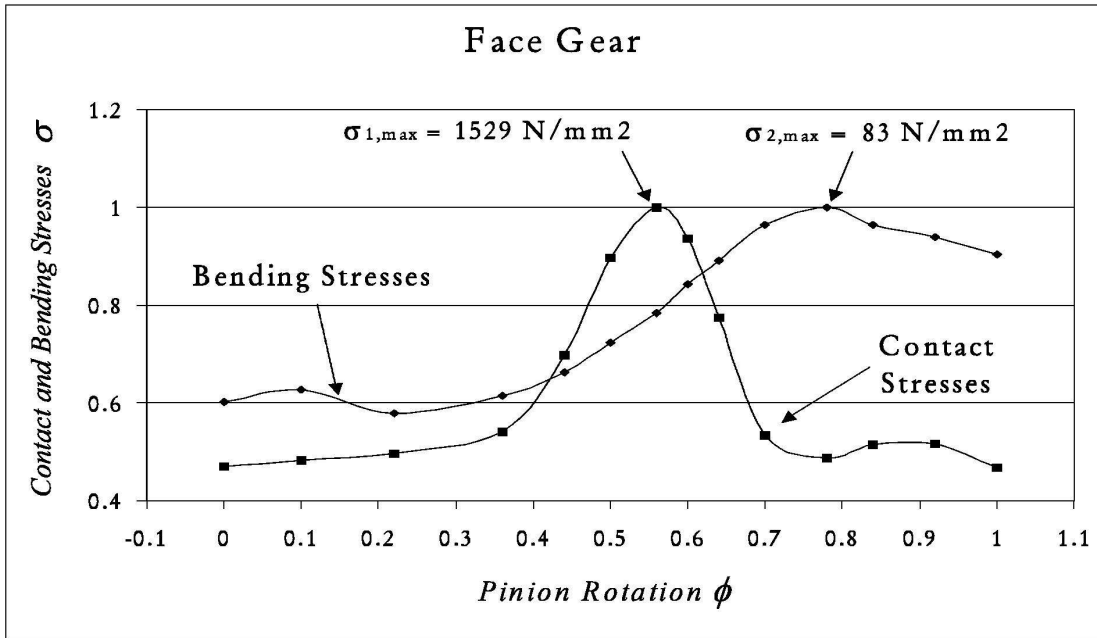
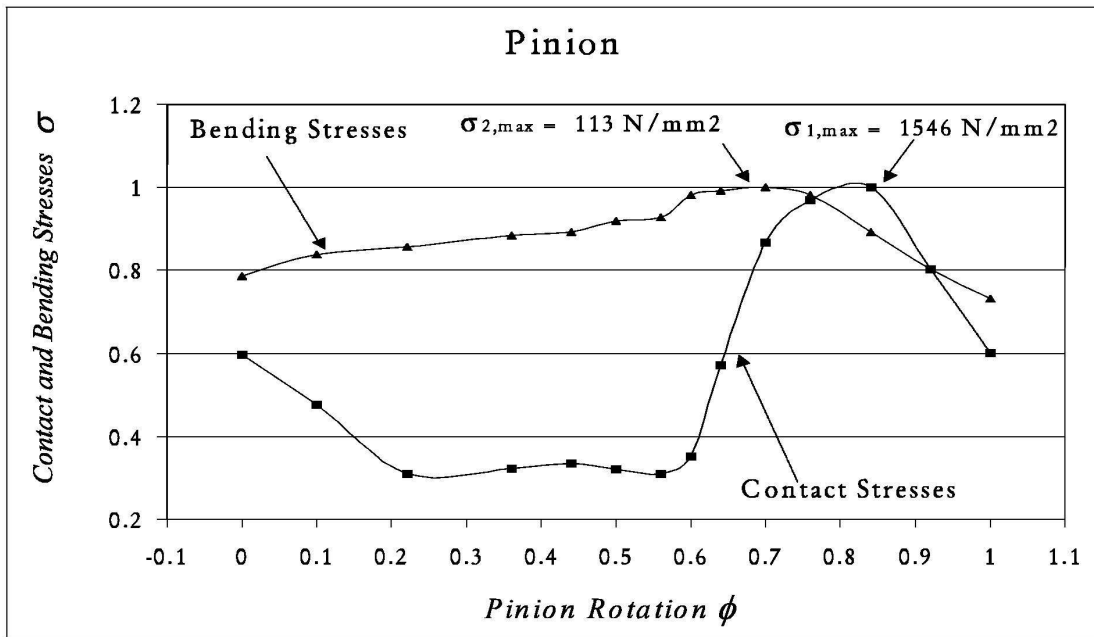


Figure 25: Contact and bending stresses for version 2 of face-gear drive



(a)



(b)

Figure 26: Variation of functions of contact and bending stresses during the cycle of meshing for (a) the face-gear and (b) the pinion

<b>REPORT DOCUMENTATION PAGE</b>			<i>Form Approved</i> <i>OMB No. 0704-0188</i>	
Public reporting burden for this collection of information is estimated to average 1 hour per response, including the time for reviewing instructions, searching existing data sources, gathering and maintaining the data needed, and completing and reviewing the collection of information. Send comments regarding this burden estimate or any other aspect of this collection of information, including suggestions for reducing this burden, to Washington Headquarters Services, Directorate for Information Operations and Reports, 1215 Jefferson Davis Highway, Suite 1204, Arlington, VA 22202-4302, and to the Office of Management and Budget, Paperwork Reduction Project (0704-0188), Washington, DC 20503.				
<b>1. AGENCY USE ONLY (Leave blank)</b>		<b>2. REPORT DATE</b> February 2002	<b>3. REPORT TYPE AND DATES COVERED</b> Final Contractor Report	
<b>4. TITLE AND SUBTITLE</b> Face Gear Drive With Spur Involute Pinion: Geometry, Generation by a Worm, Stress Analysis			<b>5. FUNDING NUMBERS</b>  WU-728-30-10-00 NAG3-2450 1L162211A47A	
<b>6. AUTHOR(S)</b>  Faydor L. Litvin, Alfonso Fuentes, Claudio Zanzi, and Matteo Pontiggia				
<b>7. PERFORMING ORGANIZATION NAME(S) AND ADDRESS(ES)</b> University of Illinois at Chicago Gear Research Center Department of Mechanical Engineering Chicago, Illinois 60607			<b>8. PERFORMING ORGANIZATION REPORT NUMBER</b>  E-13183	
<b>9. SPONSORING/MONITORING AGENCY NAME(S) AND ADDRESS(ES)</b> National Aeronautics and Space Administration Washington, DC 20546-0001 and U.S. Army Research Laboratory Adelphi, Maryland 20783-1145			<b>10. SPONSORING/MONITORING AGENCY REPORT NUMBER</b>  NASA CR-2002-211362 ARL-CR-491	
<b>11. SUPPLEMENTARY NOTES</b>  Project Manager, Robert F. Handschuh, U.S. Army Research Laboratory, NASA Glenn Research Center, 216-433-3969.				
<b>12a. DISTRIBUTION/AVAILABILITY STATEMENT</b> Unclassified - Unlimited Subject Category: 37 Available electronically at <a href="http://gltrs.grc.nasa.gov/GLTRS">http://gltrs.grc.nasa.gov/GLTRS</a> This publication is available from the NASA Center for AeroSpace Information, 301-621-0390.			<b>12b. DISTRIBUTION CODE</b>	
<b>13. ABSTRACT (Maximum 200 words)</b>  A face gear drive with a spur involute pinion is considered. The generation of the face gear is based on application of a grinding or cutting worm whereas the conventional method of generation is based on application of an involute shaper. An analytical approach for determination of: (i) the worm thread surface, (ii) avoidance of singularities of the worm thread surface, (iii) dressing of the worm, and (iv) determination of stresses of the face-gear drive, is proposed. A computer program for simulation of meshing and contact of the pinion and face-gear has been developed. Correction of machine-tool settings is proposed for reduction of the shift of the bearing contact caused by misalignment. An automatic development of the model of five contacting teeth has been proposed for stress analysis. Numerical examples for illustration of the developed theory are provided.				
<b>14. SUBJECT TERMS</b>  Gears; Transmissions			<b>15. NUMBER OF PAGES</b> 50	
			<b>16. PRICE CODE</b>	
<b>17. SECURITY CLASSIFICATION OF REPORT</b> Unclassified	<b>18. SECURITY CLASSIFICATION OF THIS PAGE</b> Unclassified	<b>19. SECURITY CLASSIFICATION OF ABSTRACT</b> Unclassified	<b>20. LIMITATION OF ABSTRACT</b>	